

Article

Catalytic Fast Pyrolysis of Lignin Isolated by Hybrid Organosolv—Steam Explosion Pretreatment of Hardwood and Softwood Biomass for the Production of Phenolics and Aromatics

Ioannis Charisteidis ¹, Polykarpos Lazaridis ¹, Apostolos Fotopoulos ¹, Eleni Pachatouridou ², Leonidas Matsakas ³ , Ulrika Rova ³ , Paul Christakopoulos ^{3,*} and Konstantinos Triantafyllidis ^{1,*}

¹ Department of Chemistry, Aristotle University of Thessaloniki, 54124 Thessaloniki, Greece; icharisteidis@gmail.com (I.C.); lazaridp@chem.auth.gr (P.L.); afotopou@auth.gr (A.F.)

² Chemical Process and Energy Resources Institute, Centre for Research and Technology-Hellas (CPERI/CERTH), 57001 Thessaloniki, Greece; e_pahat@cperi.certh.gr

³ Biochemical Process Engineering, Division of Chemical Engineering, Department of Civil, Environmental and Natural Resources Engineering, Luleå University of Technology, 971-87 Luleå, Sweden; leonidas.matsakas@ltu.se (L.M.); Ulrika.Rova@ltu.se (U.R.)

* Correspondence: ktrianta@chem.auth.gr (K.T.); paul.christakopoulos@ltu.se (P.C.)

Received: 11 October 2019; Accepted: 2 November 2019; Published: 8 November 2019



Abstract: Lignin, one of the three main structural biopolymers of lignocellulosic biomass, is the most abundant natural source of aromatics with a great valorization potential towards the production of fuels, chemicals, and polymers. Although kraft lignin and lignosulphonates, as byproducts of the pulp/paper industry, are available in vast amounts, other types of lignins, such as the organosolv or the hydrolysis lignin, are becoming increasingly important, as they are side-streams of new biorefinery processes aiming at the (bio)catalytic valorization of biomass sugars. Within this context, in this work, we studied the thermal (non-catalytic) and catalytic fast pyrolysis of softwood (spruce) and hardwood (birch) lignins, isolated by a hybrid organosolv–steam explosion biomass pretreatment method in order to investigate the effect of lignin origin/composition on product yields and lignin bio-oil composition. The catalysts studied were conventional microporous ZSM-5 (Zeolite Socony Mobil-5) zeolites and hierarchical ZSM-5 zeolites with intracrystal mesopores (i.e., 9 and 45 nm) or nano-sized ZSM-5 with a high external surface. All ZSM-5 zeolites were active in converting the initially produced via thermal pyrolysis alkoxy-phenols (i.e., of guaiacyl and syringyl/guaiacyl type for spruce and birch lignin, respectively) towards BTX (benzene, toluene, xylene) aromatics, alkyl-phenols and polycyclic aromatic hydrocarbons (PAHs, mainly naphthalenes), with the mesoporous ZSM-5 exhibiting higher dealkoxylation reactivity and being significantly more selective towards mono-aromatics compared to the conventional ZSM-5, for both spruce and birch lignin.

Keywords: spruce and birch wood lignin; hybrid organosolv—steam explosion pretreatment; catalytic fast pyrolysis; model compounds; bio-oil; phenolics and aromatics; microporous and hierarchical ZSM-5 zeolite

1. Introduction

Lignocellulosic biomass is nowadays considered to be an important renewable source for the production of fuels, energy, chemicals, polymers, and other products, with the (bio)catalytic processes playing a major role [1–4]. Lignocellulose comprises of two polysaccharides, cellulose (30–50 wt.%) and hemicellulose (15–30 wt.%), and an amorphous phenolic polymer, lignin (10–30 wt.%) [3,5–7].

Lignin is formed via dehydrogenative polymerization of three phenylpropane units (monolignols), i.e., sinapyl, coniferyl, and p-coumaryl alcohols, which are linked via ether and C–C bonds and correspond to the syringyl (S), guaiacyl (G), and p-hydroxyphenyl (H) building blocks in the structure of lignin, respectively [8–14]. The most abundant types of bonds in lignin structures are ether type linkages, like β -O-4 (40%–50%), and others, such as α -O-4, 5-5, β -5, β -1, dibenzodioxocin, spirodienone, and β - β linkages [8,10,15]. The composition and structure of lignin depend on the type and nature of plant biomass. Softwoods, such as spruce, pine, etc., contain 20 to 30 wt.% lignin, hardwoods, such as birch, beech, poplar, etc. 15 to 25 wt.%; and grasses, straw, and stover 10 to 20 wt.%. Likewise, softwood-derived lignins contain mainly coniferyl alcohol units, i.e., guaiacyl units. Hardwood lignins comprise of both guaiacyl and syringyl (sinapyl alcohol) (S) units, the latter having two methoxy groups, while lignin from grass also contains p-hydroxyphenyl (p-coumaryl alcohol) units in addition to G and S units [9,10,16].

Lignin is typically produced in vast amounts as a low value byproduct in the traditional pulp and paper industry (i.e., kraft and sulphite lignin) and is mainly utilized to generate heat and power through combustion. In more recent years, lignin has also been utilized in various sectors, such as an asphalt emulsifier, dispersant for clays, dyestuffs, insecticides, adhesive resins, soil upgrading agent, rubber reinforcing agent, adsorbent, biochar and carbon fibers, grinding agent for cement, viscosity reducer of heavy oil, surface active agent for oil extraction, lubricant additive, vanillin production, etc. [14,17–22]. In addition to the above classical technical lignins, the emerging biorefinery concept in recent years has generated the need for more efficient, sustainable, and environment-friendly biomass fractionation processes that will facilitate downstream conversion of carbohydrates and lignin to value-added products. For example, in the production of second-generation bioethanol, i.e., by utilizing lignocellulosic, mainly residual/waste, biomass, the initial pretreatment step is very important and aims to maximize the enzymatic hydrolysis of cellulose to glucose, which is then fermented to ethanol [23]. Within this context, two types of pretreatment have attracted increased interest due to their efficiency combined with green process characteristics, i.e., the hydrothermal (liquid hot water) [24–26] or steam explosion pretreatment [27–29] utilizing neat water/steam and the organosolv process [30–32] that uses mixtures of water with friendly solvents (i.e., ethanol) under relatively mild hydrothermal conditions (i.e., up to ca. 200 °C). Moreover, extraction of surface lignin with acetone and ethanol from hydrothermally pretreated biomass has recently been proposed as a method to overcome inhibitory effects imposed by lignin during enzymatic hydrolysis of cellulose [26]. With regard to the organosolv pretreatment, it was shown that the use of small amounts of acids (i.e., H₂SO₄ or H₃PO₄) may further improve the efficiency of the process [30,33]. More recently, a hybrid organosolv–steam explosion process was proposed for the pretreatment and efficient fractionation of biomass, leading to enhanced enzymatic hydrolysis and isolation of high-quality and purity lignin [34,35]. For example, by pretreating birch and spruce biomass with this method, solids with high cellulose (77.9 wt.% and 72 wt.%, respectively) and low lignin (delignification up to 86.2 wt.% and 79.4 wt.%, respectively) content were obtained. These solids exhibited high saccharification activity (yields up to 61% w/w for spruce and complete saccharification for birch), thus rendering them as ideal feedstocks for downstream (bio)catalytic valorization [34,35].

With regard to lignin depolymerization and further upgrading to phenolic and aromatic compounds, two of the most studied methods are catalytic hydrogenolysis and fast pyrolysis. The former usually takes place at low/moderate reaction temperatures (ca. 150–350 °C) under high H₂ pressure (ca. 20–90 bar) and/or by using solvents that can act as hydrogen donors, in a neutral, basic, or acidic environment [36]. The most common catalysts comprise of noble and transition metals (i.e., Ru, Pd, Pt, Ni, Cu, etc.) supported on carbons, carbides, zeolites, and various oxides that are aimed at the scission of C–O (e.g., β -O-4 bonds) and C–C bonds towards the production of smaller phenolic fragments or phenolic, aromatic, and alkane monomers [8,37–42]. Fast pyrolysis is a thermochemical process that takes place at moderate/high temperatures of ca. 400 to 700 °C in the absence of oxygen/air. The process characteristics, i.e., fast heating and cooling rates, moderate

temperatures, and short vapor contact times, favor the formation of a liquid product called bio-oil. In the case of lignin, the bio-oil mainly contains alkoxy-phenols and oxygenated aromatics, such as syringol, guaiacol, and their alkylated analogues, vanillin, syringaldehyde, 1,2,3-trimethoxy-benzene, and others. The composition of bio-oil is dependent on the origin of the lignin, i.e., the type of lignocellulosic biomass. Furthermore, it was recently shown that the composition of lignin, i.e., the type of building units, is depicted in the composition of the bio-oil, i.e., the bio-oil produced from a kraft softwood (spruce) lignin that was enriched in guaiacyl units contained only guaiacol-type (with one methoxy group) compounds [43]. Some gases, such as carbon dioxide, carbon monoxide, and methane, as well as solids (char), are also produced in lignin fast pyrolysis; the latter being in higher yields (ca. 40–50 wt.%) compared to the char produced in biomass fast pyrolysis (ca. 15–25 wt.%) [10,44–47]. Due to its phenolic nature and the relatively high homogeneity compared to the parent biomass fast pyrolysis oil, which in addition to phenolic compounds also contains furans, acids, esters, ketones, aldehydes, ethers, alcohols, and sugars due to cellulose/hemicellulose pyrolysis, lignin-derived bio-oil could be utilized in the production of phenol-based resins and polyurethanes, replacing petroleum phenol [48,49]. Furthermore, it can be subjected to hydrodeoxygenation (HDO) for the production of aromatics and cycloalkanes [50–55].

An alternative method for the deoxygenation of lignin bio-oil, avoiding the use of hydrogen, is the catalytic fast pyrolysis (CFP) of lignin, in analogy to the CFP of lignocellulosic biomass, where the initially produced biomass thermal pyrolysis vapors are further converted (in situ or ex situ) on the catalyst active sites [56–60]. Although different types of catalysts, i.e., acidic, basic, metal oxides, bifunctional metal-acidic, etc., have been studied in biomass CFP, leading to varying degrees of deoxygenation and bio-oil composition, the use of zeolites, mainly ZSM-5, induces deep deoxygenation via enhanced dehydration, decarbonylation, and decarboxylation reactions. Further transformation of the intermediate products via cracking, (de)alkylation, isomerization, aromatization, condensation, and oligomerization reactions on the zeolitic catalysts results in the production of a highly deoxygenated bio-oil that consists mainly of monocyclic aromatic hydrocarbons (i.e., benzene, toluene, xylenes, etc.), naphthalenes, and alkyl-phenols. The penalty is the increased production of water (aqueous fraction of bio-oil) and gases, as well as catalytic coke, at the expense of the organic fraction of bio-oil [57,60–64]. Similar effects have been observed in the case of lignin CFP, where the use of zeolitic catalysts, including ZSM-5, beta, mordenite, ferrierite, and USY (Ultra Stable Y), has mainly been investigated [43,63,65–70]. ZSM-5 has been shown to be very reactive towards aromatic compounds, due to its unique microporous structure and strong Brønsted acidity; however, USY zeolite, which possesses larger micropores than those of ZSM-5 zeolite, has also been shown to be quite efficient in the production of hydrocarbons, also exhibiting a relatively low formation of tar [68]. More recently, it has also been shown that nano-sized Al-MCM-41 mesoporous catalysts may exhibit a similar deoxygenation activity and yield of aromatics compared to strongly acidic microporous ZSM-5 zeolite in fast pyrolysis of alkali softwood lignin [71].

A more recent type of zeolitic catalysts, the so-called hierarchical zeolites, which exhibit both the improved diffusion properties of mesoporous materials and the strong acidity and stability of zeolites [72–74], has also been investigated in biomass CFP [75–81]. However, few studies have been reported so far on lignin CFP. In the work of Lee et al., it was shown that the production of mono-aromatics and polycyclic aromatic hydrocarbons (PAHs) with a mesoporous Y zeolite (prepared from USY) was substantially improved compared to a conventional Al-MCM-41, which mostly produced phenolics [82]. Li et al. compared a typical microporous ZSM-5 zeolite with an alkaline-treated mesoporous ZSM-5 and showed that with the latter catalyst, both aromatics and phenols were increased while the yield of char/coke was decreased [83]. Kim et al. compared a mesoporous MFI zeolite with an Al-SBA-15 mesoporous aluminosilicate and reported an enhanced formation of alkyl-phenols and mono-aromatics due to the strong Brønsted acidity of the mesoporous zeolite [84]. More recently, in our previous work, the catalytic fast pyrolysis of a kraft (softwood) lignin with different ZSM-5-based catalysts was shown, including a mesoporous ZSM-5 and a nano-sized ZSM-5 [43]. It was shown that the classical microporous ZSM-5 zeolites were slightly more selective

towards mono-aromatics while the nano-sized and especially the mesoporous ZSM-5 exhibited, in addition to aromatics, a high selectivity towards alkyl-phenols. Furthermore, the nano-sized ZSM-5 induced lower yields of the organic bio-oil fraction and higher production of water, coke, and gases in comparison to the micro- and mesoporous ZSM-5 zeolites.

Within this context, in this work, we studied the thermal (non-catalytic) and catalytic fast pyrolysis of softwood (spruce) and hardwood (birch) lignins, isolated by the recently proposed organosolv—steam explosion pretreatment method [34,35], in order to further investigate the effect of lignin origin/composition on the product yields and lignin oil composition. Furthermore, the fast pyrolysis of two model compounds, i.e., guaiacol and syringol, was also investigated in order to elucidate possible reaction pathways in lignin pyrolysis. The catalysts studied were two microporous ZSM-5 zeolites with an Si/Al ratio equal to 11.5 and 40, meso-ZSM-5 zeolites with intra-crystal mesoporosity and different mesopore sizes (i.e., 9 and 45 nm) produced by alkaline treatment of commercial ZSM-5, as well as a nano-ZSM-5 zeolite produced by hydrothermal synthesis. Two pyrolysis set-ups were used, a pyrolyzer/gas chromatography-mass spectrometry (Py/GC-MS) system and a bench scale fast pyrolysis unit with a fixed bed reactor, while the obtained catalytic data were correlated and discussed in light of the catalysts' textural and acidic characteristics, as well as the feed lignin properties.

2. Results and Discussion

2.1. Lignin Characteristics

The elemental analysis of the spruce- and birch-derived lignin samples, isolated by the hybrid organosolv—steam explosion method, and used as feedstock in the fast pyrolysis experiments is shown in Table 1. The content of C, H, and O was typical for this type of lignin while S and N contents were also very low [85–88]. The low content of S, as well as of inorganic ash, is a beneficial characteristic of organosolv-type lignins with regard to their valorization, compared, for example, to kraft lignin and liginosuphonates [43,67,89]. The spruce and birch lignins used in this study, which were isolated by the hybrid organosolv—steam explosion method, contained a very low amount of ash (<0.1 wt.%), as well as minimal carbohydrate impurities, i.e., hemicellulose (<2 wt.%) and cellulose (<1 wt.%) [34,35]. Their molecular weights were also in the range of previously reported values for similar organosolv-type lignins, with a relatively narrow molecular mass distribution as evidenced by the low polydispersity index (PDI) values [22,85,87,90,91].

Table 1. Physicochemical characteristics of spruce- and-birch derived lignin isolated by the hybrid organosolv—steam explosion pretreatment.

Lignin Sample	C (wt.%)	H (wt.%)	S (wt.%)	N (wt.%)	O ¹ (wt.%)	Ash (wt.%)	Mn (g/mol)	Mw (g/mol)	PDI
Spruce Lignin	64.74	6.25	0.01	0.45	28.55	0.10	1017 [90]	2832 [90]	2.79 [90]
Birch Lignin	62.86	6.54	0.02	0.50	30.08	0.17	1624 [22]	4414 [22]	2.72 [22]

¹ Calculated by difference.

The thermal decomposition profile of both lignins is depicted in the thermogravimetric analysis (TGA) and differential thermogravimetric analysis (DTG) curves shown in Figure 1. The initial weight loss of ~2% up to ca. 120 °C is due to the evaporation of humidity while the steep weight loss of ~51% for spruce lignin (DTG maximum 398 °C) and ~60% for birch lignin (DTG maximum 354 °C), in the range of ca. 180 to 600 °C, is attributed to the decomposition of lignin. The above differences in the weight loss and DTG maxima indicate the relatively higher stability of spruce-derived lignin. A further progressive limited weight loss was observed at higher temperatures, which can be attributed to enhanced condensation reactions and/or gasification of the formed carbonaceous material. The higher residual char at 950 °C produced by spruce lignin (~32%) compared to birch lignin (~25%) can also be related

to the higher thermal stability of the former, as well as to enchanted repolymerization/condensation reactions that occur under the slow pyrolysis conditions of the TGA experiment.

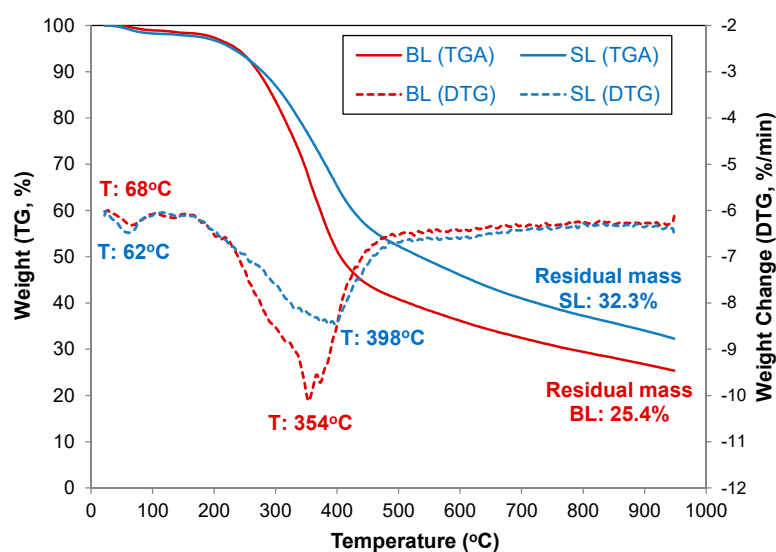


Figure 1. TGA and DTG curves of the spruce (SL) and birch (BL) lignins isolated by organosolv—steam explosion pretreatment.

The spruce and birch lignins, isolated by the hybrid organosolv—steam explosion method, were also characterized by 2D HSQC (Heteronuclear Single Quantum Coherence) NMR and the respective spectra that correspond to the inter-unit linkages and the types of aromatic units are shown in Figure 2. The HSQC cross peaks were attributed to specific aromatic units and linkages using previously reported data [92–98]. The assigned peaks are listed in Table 2 and the specific types of aromatic units (S, S', G, G', H) and inter-unit linkages (A, B, C, I, J, FA) are shown in Figure 3. The HSQC spectrum referring to the aromatic units of spruce lignin (Figure 2a; δ_C/δ_H 100–155/6.3–7.7 ppm) clearly shows that this lignin consists only of guaiacyl (G) units, as was expected due to the nature of spruce being a softwood. As a specific case of the guaiacyl units, a ferulate structure (FA structure) seems to be present to some extent (4.8 units per 100 Ar) since the C_2-H_2 and C_6-H_6 correlation peaks of the ferulate end-groups appear in the spectrum at δ_C/δ_H 111.2/7.35 ppm and 123.6/7.19 ppm, respectively. In this part of the spectrum, there are also two peaks at δ_C/δ_H 153.7/7.65 ppm and 125.9/7.0 ppm that correspond to the α and β atom of an aldehyde end-group (J structure, 4.5 units per 100 Ar). On the other hand, the HSQC spectrum of birch lignin (Figure 2c; δ_C/δ_H 100–155/5.9–7.9 ppm) shows that this lignin consists mainly of syringyl (S) lignin units. A lesser amount of guaiacyl (G) units and a small quantity of p-hydroxyphenyl structures (H units) is also present. Integrating the respective cross-peaks, the molar ratio of the S, G, and H units for the birch lignin was found to be S/G/H = 77.0/22.3/0.7%. Apart from the main lignin units, in this part of the birch lignin spectrum, there is evidence of some amounts of an aldehyde end-group (J structure, 2.9 groups per 100 Ar) with its $C_\alpha-H_\alpha$ correlation peak at δ_C/δ_H 153.7/7.65 ppm and a ferulate structure (FA structure, 0.7 groups per 100 Ar) with its C_2-H_2 correlation peak at δ_C/δ_H 111.2/7.35 ppm. Small amounts of xylan were observed at δ_C/δ_H 72.5/3.07 ppm (X_2 atom of xylan structure, 3.3 groups per 100 Ar) and δ_C/δ_H 74.75/3.55 ppm (X_4 atom of xylan structure, 1.6 groups per 100 Ar) [92,97]. The cross-peak at δ_C/δ_H 131.4/6.47 ppm can be ascribed to the $C_\alpha-H_\alpha$ correlation peak of a not common structure that contains a conjugated double bond [94].

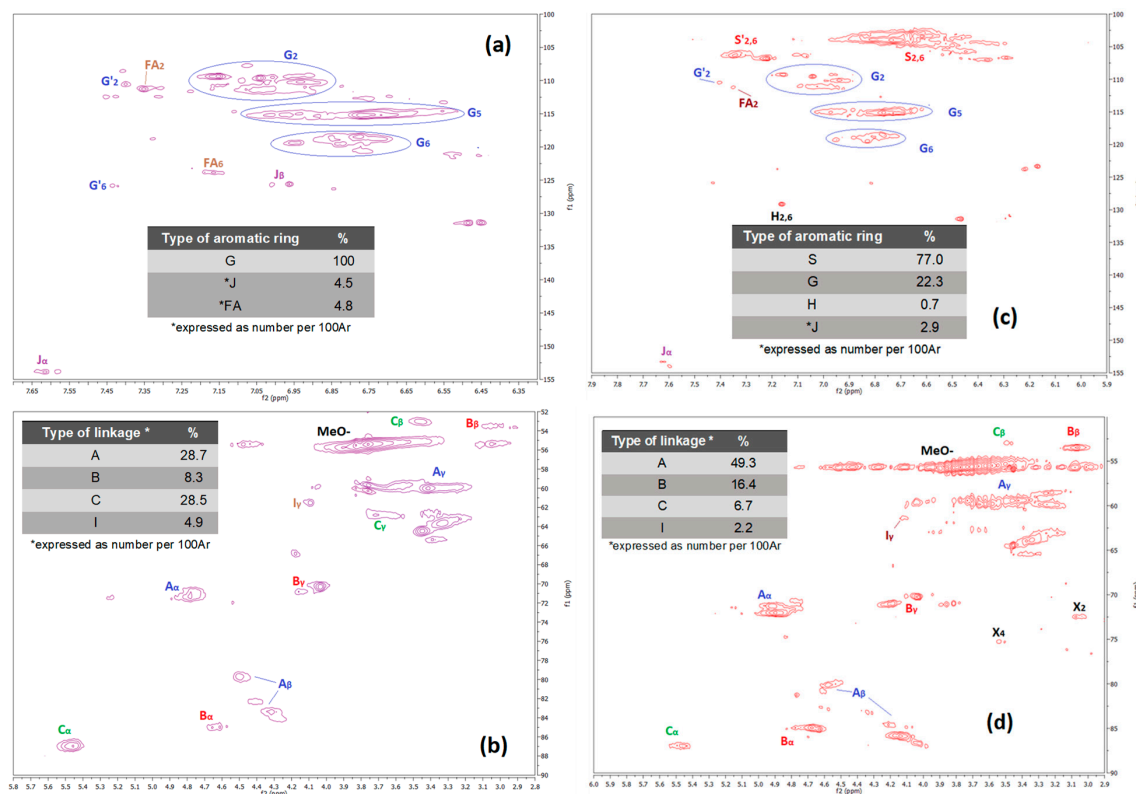


Figure 2. 2D HSQC spectra of spruce lignin (a,b) and birch lignin (c,d), isolated by the hybrid organosolv—steam explosion method: (a,c) aromatic structures, and (b,d) inter-unit linkages.

Table 2. List of assigned HSQC cross-peaks of the spruce- and birch-derived lignins.

Label	δ_C/δ_H (ppm)	Assignment
B $_{\beta}$	53.5/3.07	C $_{\beta}$ -H $_{\beta}$ in resinol substructures (B)
A $_{\gamma}$	59.4–60.0/3.2–3.8	C $_{\gamma}$ -H $_{\gamma}$ in β -O-4' substructures (A)
C $_{\gamma}$	62.8/3.74	C $_{\gamma}$ -H $_{\gamma}$ in phenylcoumaran substructures (C)
I $_{\gamma}$	61.4/4.13	C $_{\gamma}$ -H $_{\gamma}$ in alcohol end-groups (I)
B $_{\gamma}$	70.3–71.0/4.04–4.18	C $_{\gamma}$ -H $_{\gamma}$ in resinol substructures (B)
A $_{\alpha}$	71.2–72.0/4.78–4.92	C $_{\alpha}$ -H $_{\alpha}$ in β -O-4' substructures (A)
X $_2$	72.5/3.07	C $_2$ -H $_2$ in xylan substructures (X)
X $_4$	75.3/3.54	C $_4$ -H $_4$ in xylan substructures (X)
A $_{\beta}$	80.1–86.6/4.03–4.50	C $_{\beta}$ -H $_{\beta}$ in β -O-4' substructures (A)
B $_{\alpha}$	84.9–8.51/4.63–4.68	C $_{\alpha}$ -H $_{\alpha}$ in β - β resinol (B)
C $_{\alpha}$	87.0/5.45	C $_{\alpha}$ -H $_{\alpha}$ in phenylcoumaran substructures (C)
S $_{2,6}$	103.4–104.0/6.50–6.81	C $_{2,6}$ -H $_{2,6}$ in syringyl units (S)
S' $_{2,6}$	106.3–106.8/7.22–7.35	C $_{2,6}$ -H $_{2,6}$ in oxidized (C $_{\alpha}$ =O) syringyl units (S')
G $_2$	109.4–111.3/6.94–7.15	C $_2$ -H $_2$ in guaiacyl units (G)
G' $_2$	110.5/7.40	C $_2$ -H $_2$ in oxidized (C $_{\alpha}$ =O) guaiacyl units (G')
FA $_2$	111.2/7.35	C $_2$ -H $_2$ in ferulates (FA)
G $_5$	115.1–115.2/6.73–6.97	C $_5$ -H $_5$ in guaiacyl units (G)
G $_6$	118.4–119.5/6.76–6.96	C $_6$ -H $_6$ in guaiacyl units (G)
FA $_6$	123.8/7.17	C $_6$ -H $_6$ in ferulates (FA)
J $_{\beta}$	125.6–126.3/6.84–6.96	C $_{\beta}$ -H $_{\beta}$ in aldehyde end-groups (J)
G' $_6$	125.9/7.44	C $_6$ -H $_6$ in oxidized (C $_{\alpha}$ =O) guaiacyl units (G')
H $_{2,6}$	129.1/7.16	C $_{2,6}$ -H $_{2,6}$ in p-hydroxyphenyl units (H)
J $_{\alpha}$	153.8–154.0/7.60–7.67	C $_{\alpha}$ -H $_{\alpha}$ in aldehyde end-groups (J)

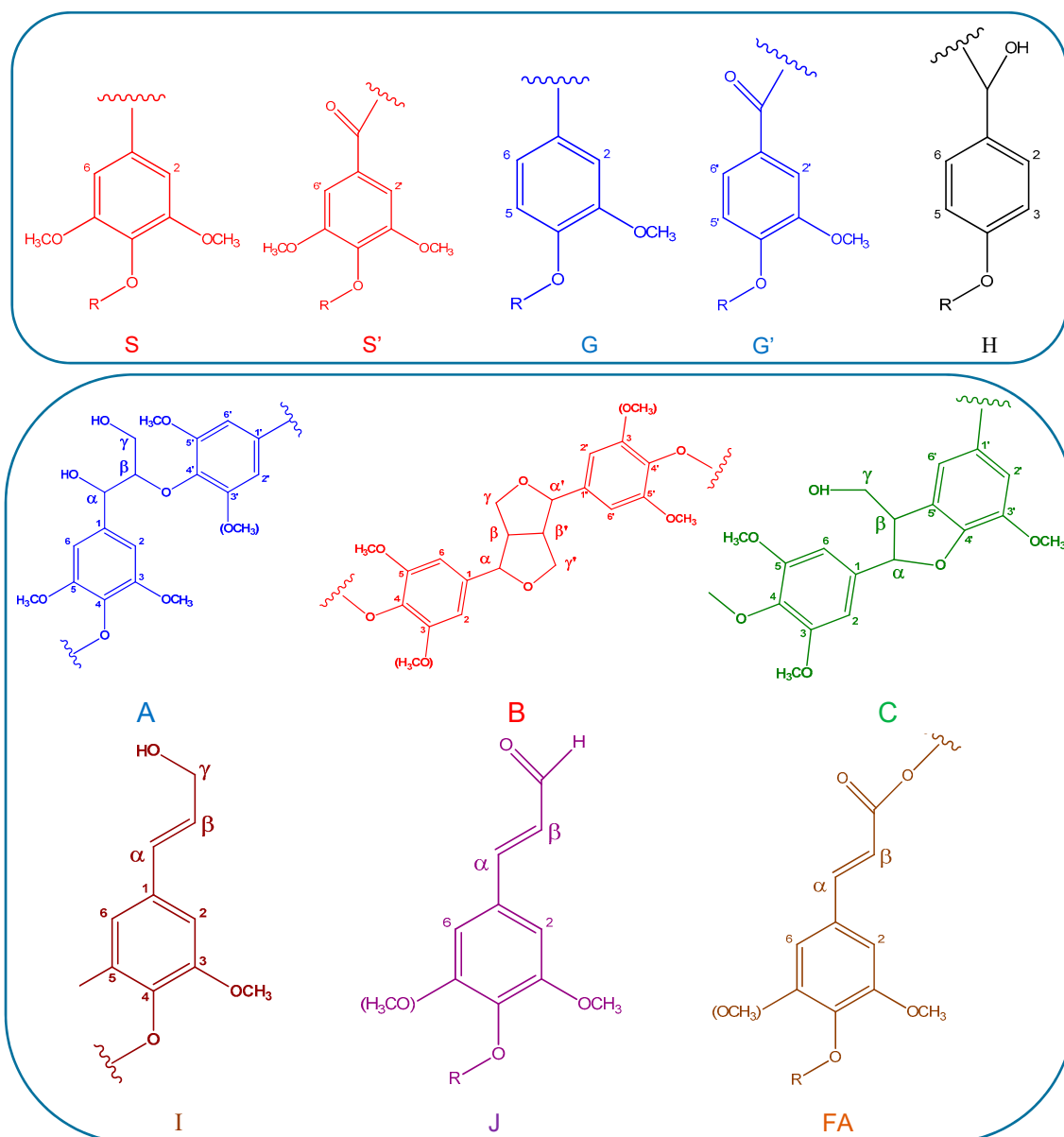


Figure 3. Types of aromatic units (upper frame) and types of linkages and end-groups (lower frame), identified by the 2D HSQC measurements in the birch- and spruce-isolated lignins.

The part of the HSQC spectrum referring to inter-unit linkages for spruce lignin (Figure 2b; δ_C/δ_H 52–90/2.8–5.8 ppm) is dominated by the strong signals of both the phenylcoumaran structures (β -5', type C linkage, 28.5 bonds per 100 Ar) and β -Aryl ethers (β -O-4', type A linkage, 28.7 bonds per 100 Ar) while pinoresinols (β - β' , type B linkage, 8.3 bonds per 100 Ar) exist in small amounts. The relative abundance of each type of linkage was found as $A/B/C = 28.7/8.3/28.5\%$ by integration of the respective peaks. Apart from these main types of linkages, in this part of the spectrum, the presence of an alcohol end-group (I structure, 4.9 groups per 100 Ar) is evidenced by its C_γ - H_γ correlation peak that appears at 61.4/4.10 ppm. In the respective part of the birch lignin HSQC spectrum (Figure 2d; δ_C/δ_H 50–90/2.9–6.0 ppm), the main type of inter-unit linkages is that of β -aryl ethers (β -O-4', type A linkage, 49.3 units per 100 Ar) while there is also a substantial quantity of pinoresinols (β - β' , type B linkage, 16.4 units per 100 Ar) and a small amount of phenylcoumaran structures (β -5', type C linkage, 6.7 bonds per 100 Ar). The relative abundance of each type of linkage was found to be $A/B/C = 49.3/16.4/6.7\%$ by integration of the respective peaks. In this part of the spectrum, there is also a

small peak at (δ_C/δ_H 61.4/4.1 ppm) that corresponds to the γ atom of an alcohol end-group (I structure, 2.2 groups per 100 Ar).

2.2. Characterization Data of ZSM-5 Zeolites

The XRD patterns of all the ZSM-5 zeolites tested, i.e., conventional microporous, mesoporous, and nano-ZSM-5, revealed their high crystallinity and exhibited diffraction peaks that are characteristic of the MFI structure (Figure 4), as was also previously shown for similar ZSM-5 zeolite catalysts [43]. The intensity of the peaks of the mesoporous and nano-sized ZSM-5 zeolites was slightly lower, which is consistent with the related reduction in the intrinsic density and scattering power of the crystals [73]. Incomplete crystallization and limited long-range ordering also cannot be excluded for the nano-sized zeolite. The N_2 isotherms and the BJH pore size distribution curves of the catalysts can be seen in Figure 5. The microporous ZSM-5 zeolites, i.e., ZSM-5(40) and ZSM-5(11.5), exhibit I(a) adsorption isotherms based on the updated IUPAC (International Union of Pure and Applied Chemistry) classification [99], being typical for microporous zeolites (with micropores width of $< \sim 1$ nm) without significant crystal and textural imperfections that may induce secondary meso/macroporosity [43]. The typical well-formed crystals with a parallelepiped shape can be seen in the TEM images of these zeolites (Figure S1, Supplementary Material). The BET total surface area of both ZSM-5(11.5) and ZSM-5(40) zeolites is around $430 \text{ m}^2/\text{g}$ and the micropore area is ~ 330 to $350 \text{ m}^2/\text{g}$ (Table 3). The N_2 adsorption isotherm of the nano-ZSM-5 is also of type I(a), exhibiting, in addition, a steep increase of adsorbed nitrogen at high P/P_0 (≥ 0.9), which is representative of the high macropore and/or external surface area owing to inter-nanoparticle voids. This morphology can also be revealed by the SEM and TEM images of the nano-sized ZSM-5, which show the presence of primary nanocrystals of < 20 nm in size (Figure 6a), forming polycrystalline particles of up to ca. $0.5 \mu\text{m}$ (Figure 6c), which in turn are aggregated into bigger particles of 5 to $10 \mu\text{m}$ (Figure 6d).

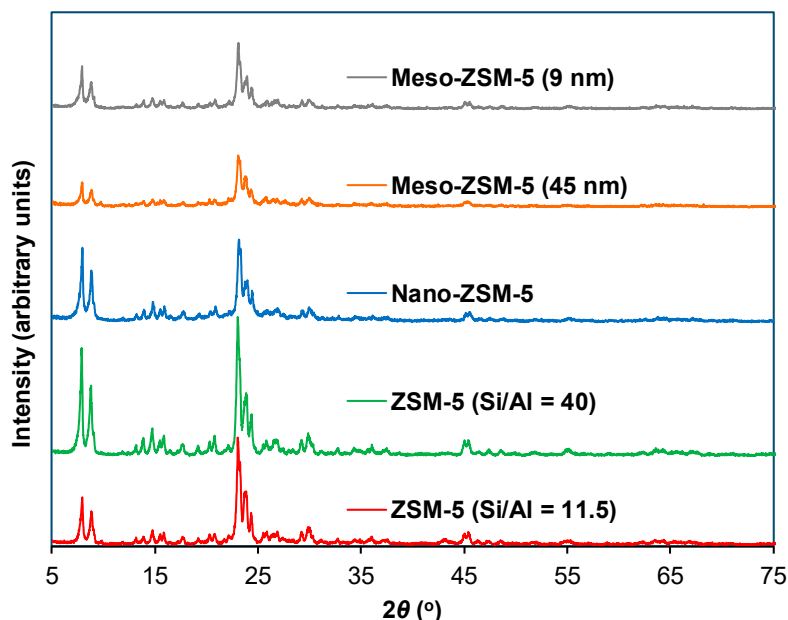


Figure 4. X-ray diffraction patterns (XRD) of commercial microporous ZSM-5 (Si/Al = 11.5, 40) zeolites, synthesized nano-sized ZSM-5, and mesoporous ZSM-5 (9 nm) and ZSM-5 (45 nm) zeolites prepared by alkaline treatment of the commercial zeolites ZSM-5 (40) and ZSM-5 (11.5), respectively.

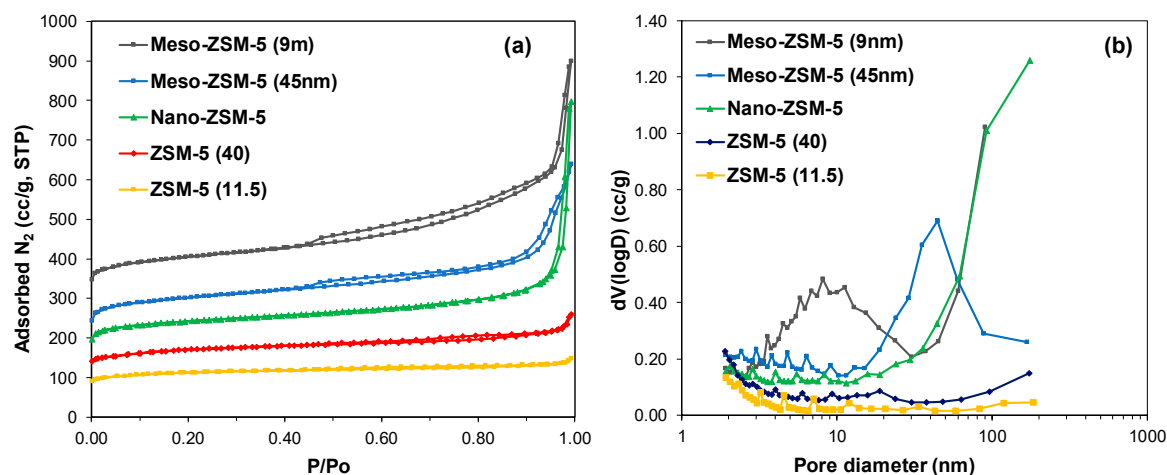


Figure 5. (a) N_2 adsorption–desorption isotherms and (b) BJH (Barrett-Joyner-Halenda) pore size distribution curves based on the adsorption data of the commercial microporous ZSM-5 (Si/Al = 11.5, 40) zeolites, the synthesized nano-sized ZSM-5 zeolite, and the mesoporous ZSM-5 (9 nm) and ZSM-5 (45 nm) zeolites prepared by mild alkaline treatment of the commercial zeolites ZSM-5 (40) and ZSM-5 (11.5), respectively; N_2 isotherms of ZSM-5 (40), nano-ZSM-5, meso-ZSM-5 (45 nm), and meso-ZSM-5 (9 nm) are shifted upwards by 50, 100, 150, and 250 cc/g, respectively.

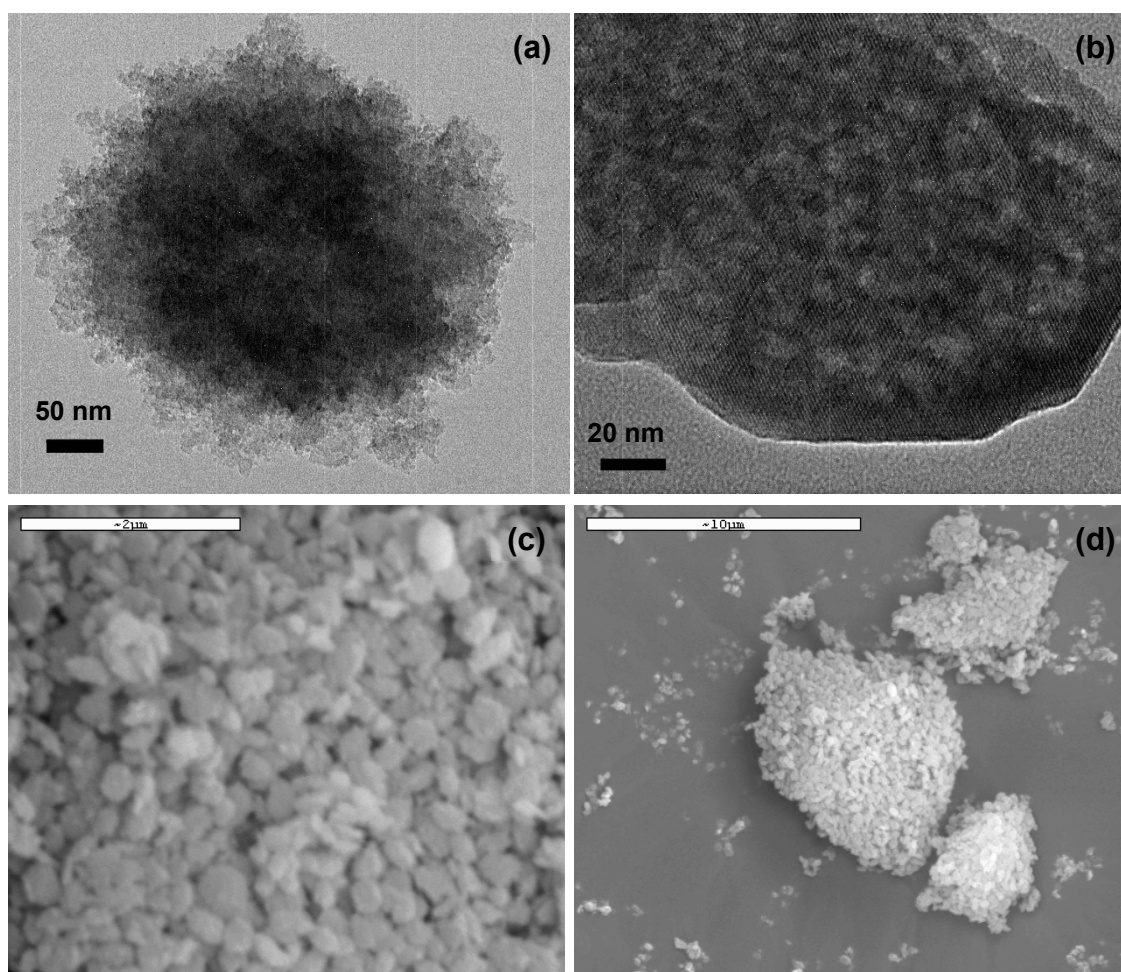


Figure 6. Transmission electron microscopy (TEM) images of (a) the nano-sized ZSM-5, and (b) the alkaline-treated mesoporous ZSM-5 (9 nm) zeolite, and scanning electron microscopy (SEM) images of the nano-sized ZSM-5 zeolite (c,d).

The N₂ adsorption isotherm of the mesoporous ZSM-5 (9 nm) zeolite that was prepared by mild alkaline treatment and subsequent washing with dilute aqueous acid solution exhibits a combined type I(a) and II, as well as a steep increase of sorbed N₂ at P/P₀ > 0.95, indicating the presence of typical zeolitic micropores, intracrystal mesopores with a broad size distribution, and increased macropore and/or external area, as was also previously shown for similar desilicated mesoporous ZSM-5 zeolite variants [43]. Indeed, in the BJH curves of Figure 5, a relatively broad pore size distribution from 2.5 to 30 nm, with a maximum at about 9 nm, can be seen for ZSM-5 (9 nm). The formation of intracrystal meso/macropores is also verified by the evenly distributed light contrast spots that can be identified in the TEM image of ZSM-5 (9 nm) (Figure 6b). Furthermore, the clearly observed zeolitic lattice fringes across the whole particle verify the high degree of crystallinity, in accordance with the XRD results. A relatively broad intra-crystal mesopore size distribution is typical for meso-ZSM-5 zeolites prepared by mild alkaline treatment of parent crystalline ZSM-5, in comparison to meso-ZSM-5 zeolites synthesized by the simultaneous use of the classical tetrapropylammonium cation (template of the MFI microporous structure) and of various mesoporous structure-directing agents [73,74,78,100]. The BET surface area of ZSM-5 (9 nm) has been significantly increased, i.e., by 28% from 437 to 560 m²/g, compared to that of the parent microporous ZSM-5 (40) zeolite, due to the substantial increase of the meso/macroporous and external area, with the simultaneous decrease of the microporous area (Table 3). This is usually observed in mesoporous ZSM-5 zeolites [73,78] and can be attributed to partial disordering of the microporous zeolitic structure especially close to the formed meso/macropores, as well as to the formation of amorphous silica-alumina impurities that block the micropores' entrance. The second mesoporous ZSM-5 sample of this study, i.e., ZSM-5 (45 nm), exhibits similar textural and porosity characteristics to ZSM-5 (9 nm), with the difference that the former zeolite contains larger mesopores in the range of 15 to 90 nm (with average width of 45 nm) (Table 3).

ZSM-5 is a strongly acidic zeolite, with many applications in the cracking/pyrolysis of petroleum or biomass-derived feedstocks, containing mainly Brønsted acid sites as well as Lewis sites when extra-framework amorphous phases are present [43,101–104]. As expected, the amount of Brønsted acid sites of the parent commercial ZSM-5 zeolites increases as the Si/Al decreases, as can be seen in Table 3. Regarding the relative strength, as can be seen in Figure 7, ZSM-5 (40) possesses stronger Brønsted acid sites compared to those of ZSM-5 (11.5). The amount of Brønsted sites and the Brønsted to Lewis (B/L) sites ratio of the meso-ZSM-5 (9 nm) remain high and similar to those of the parent ZSM-5 (40). This is indicative that the mild alkaline treatment and subsequent mild acid “washing” (for removing Na⁺ cations and formed extra-framework aluminum phases) do not significantly alter the acidic properties of ZSM-5 zeolite, as was also previously shown for similar parent and desilicated mesoporous ZSM-5 zeolite catalysts [43]. Similarly, the acidity of ZSM-5 (45 nm) has not been altered substantially (Table 3). On the other hand, the nano-sized ZSM-5 contains about half the amount of Brønsted sites, despite having a similar Al content with ZSM-5 (40) (Table 3), possibly due to the relatively lower degree of crystallinity and inadequate organization of the zeolitic framework.

Table 3. Physicochemical characteristics of various ZSM-5 zeolite catalysts.

Catalyst	BET Area ³ (m ² /g)	Micro Pore Area ⁴ (m ² /g)	Meso/Macro Pore & External Area ⁵ (m ² /g)	Average Mesopore Diameter ⁷ (nm)	Chemical Composition ⁸		Acidity ⁹		
					Al	Na	FT-IR/Pyridine (μmol Pyr/g)		
							Brønsted	Lewis	B/L
ZSM-5 (11.5)	424	349	75	-	3.20	0.06	430	123	3.5
ZSM-5 (40)	437	332	105	-	0.91	0.03	190	26	7.3
Meso-ZSM-5 (45 nm) ¹	556	289	267	44.6	2.17	0.15	384	76	5.0
Meso-ZSM-5 (9 nm) ²	560	259	301	9.0	0.82	0.05	192	21	9.1
Nano-ZSM-5	524	343	181 ⁶	-	0.86	0.08	100	53	1.9

¹ Derived from ZSM-5 (11.5) by desilication; ² Derived from ZSM-5 (40) by desilication; ³ BET surface area from N₂ sorption measurements at -196 °C using the multi-point BET method; ⁴ t-plot method; ⁵ Difference of the BET area minus the micropore area; ⁶ Attributed mainly to macropores and external surface area; ⁷ BJH analysis using adsorption data; ⁸ ICP-AES chemical analysis data; ⁹ Determination of the amount of Brønsted and Lewis acid sites by Fourier transform-infrared spectroscopy (FT-IR) combined with in situ absorption of pyridine.

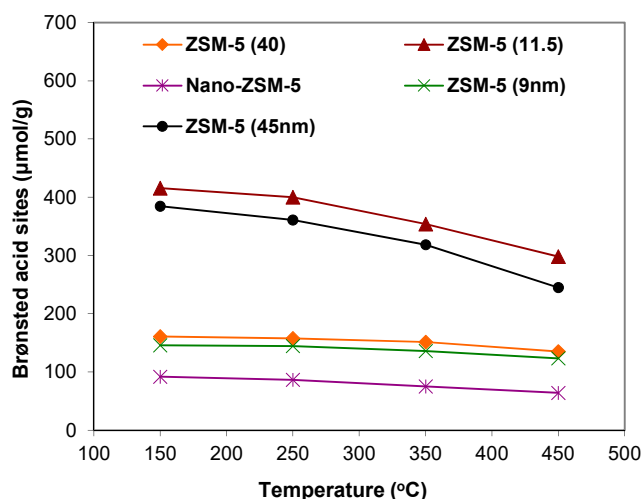


Figure 7. Amount of Brønsted acid sites of the commercial microporous ZSM-5 (Si/Al = 11.5, 40) zeolites, the synthesized nano-sized ZSM-5 zeolite, and the mesoporous ZSM-5 (9 nm) and ZSM-5 (45 nm) zeolites, as determined by FTIR-pyridine sorption measurements at increasing equilibration temperatures. Higher number of acid sites (i.e., higher amount of sorbed pyridine) retained at higher temperatures indicates higher relative acid strength of the catalyst.

2.3. Non-Catalytic and Catalytic Fast Pyrolysis of Spruce and Birch Lignins (Py/GC-MS System)

Fast pyrolysis experiments with the use of silica sand as the inert heat carrier were performed on a Py/GC-MS system at 400 and 600 °C for the spruce- and birch-derived lignins. Representative chromatograms are shown in Figure 8 while full lists of the identified compounds are given in Tables S1 and S2 for the two lignins, respectively (Supplementary Material). The distribution of the compounds among the various groups, i.e., AR, PH, OxyPH, AC, etc. (see the experimental section), is also shown in Figure 9. The spruce lignin pyrolysis vapors contained mainly alkoxy-phenolic compounds with a single alkoxy group, i.e., of the guaiacol (G) type, such as guaiacol, creosol, trans-isoeugenol, 2-methoxy-4-vinylphenol, and 4-ethyl-2-methoxy phenol, as well as guaiacol-type compounds substituted with functional groups, such as vanillin, 3-(4-hydroxy-3-methoxyphenyl)-2-propenal (coniferyl aldehyde), and 1-(4-Hydroxy-3-methoxyphenyl)-2-propanone (guaiacylacetone). A similar product distribution profile was previously observed for the fast (non-catalytic) pyrolysis of spruce kraft lignin [43], this being additional proof that the predominant G units determined by the 2D HSQC NMR measurements in the structure of softwood spruce lignin isolated either by the organosolv–steam explosion pretreatment (this study) or the kraft process are also the main components of the produced fast pyrolysis oil. Very low concentrations of other types of compounds, such as alkyl-phenols (not oxygenated), furans, acids, esters, alcohols, ethers, ketones, and oxy-aromatics, were also produced in addition to the alkoxy-phenols, as can be seen in Figure 9a and Table S1. Dimers and higher molecular weight fragments were also identified in the Py/GC-MS spectra (Figure 8a).

Due to the nature of birch (hardwood), the fast pyrolysis vapors of the isolated lignin comprised mainly of syringol (S)-type compounds with two alkoxy-groups, i.e., syringol (2,6-dimethoxy phenol) and 2,6-dimethoxy-4-(2-propenyl)-phenol; syringol-type compounds substituted with functional groups, such as 3,5-dimethoxy-acetophenone and 4-hydroxy-3,5-dimethoxy-benzaldehyde; as well as oxygenated aromatics, such as 1,2,4-trimethoxybenzene (Figure 8b and Table S2). In addition to the S-type compounds, G-type compounds were also identified, i.e., creosol, guaiacol, 4-methoxy-3-(methoxymethyl)-phenol, etc. with an S/G ratio of 70–72/30–28 at both 400 and 600 °C. As in the case of the spruce lignin, it is clear that the distribution of S and G units in birch lignin identified by 2D HSQC NMR (S/G = 77/22) was also retained in the non-catalytic fast pyrolysis oil. In addition to alkoxy-phenols, alkyl-phenols (not oxygenated), acids, ketones, oxy-aromatics, and nitrogen-containing compounds were also produced, as can be seen in Figure 9b and Table S2.

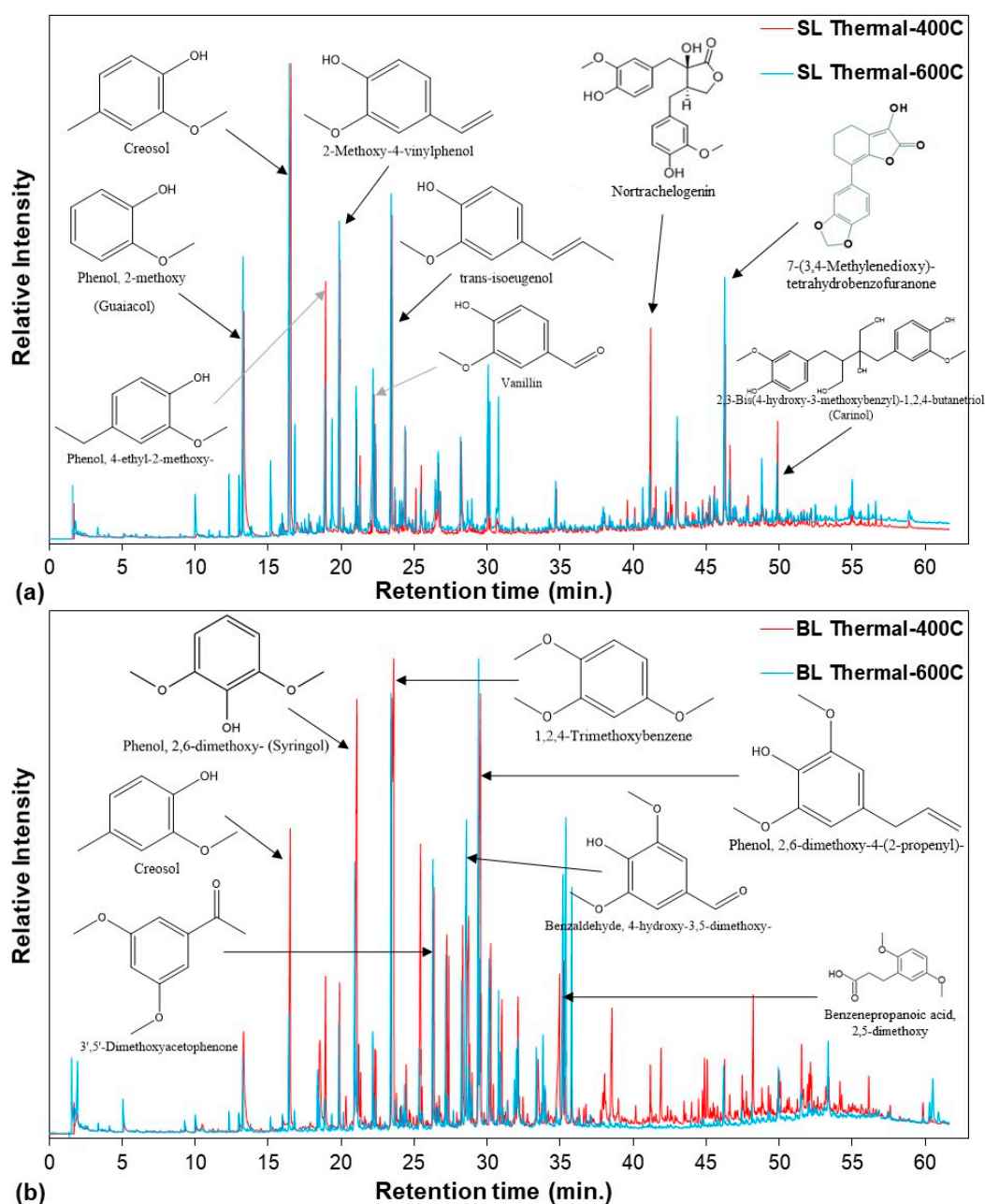


Figure 8. Representative Py/GC-MS (pyrolysis/gas chromatography-mass spectrometry) spectra of the non-catalytic (thermal) fast pyrolysis at 400 and 600 °C of: (a) spruce lignin and (b) birch lignin.

The catalytic fast pyrolysis (CFP) study on the Py/GC-MS system was performed at 600 °C with the two lignins and the ZSM-5 zeolite catalysts described in the previous section (Table 3). The temperature of 600 °C was selected for the catalytic tests in order to enhance the initial thermal decomposition of lignin towards smaller oligomers and alkoxy-phenol monomers that can further react on the catalyst. The relative abundance of the different groups of compounds can be seen in Figure 9 and a detailed list of the products is given in Tables S1 and S2 for the spruce and birch lignin, respectively. As a general trend, the use of the conventional microporous ZSM-5 zeolite in the pyrolysis of both lignins induced a substantial conversion of the initially formed (by thermal pyrolysis) alkoxy-phenols towards BTX mono-aromatics (mainly toluene, 1,3-dimethyl-benzene, 1,2,3-trimethyl-benzene, benzene, *o*-xylene, etc.), PAHs (mainly naphthalenes, such as 1- or 2-methyl-naphthalene), and alkyl-phenols (such as phenol, 2- or 3-methyl-phenol, 2,5-dimethyl-phenol, etc.) in accordance with our previous work on spruce kraft lignin pyrolysis [43] and other related studies [65,67,69,71]. The deoxygenation

activity and increased production of aromatics with ZSM-5 zeolite has been attributed to its strong Brønsted acidity and unique pore system comprising of tubular micropores of moderate size (~5.5 Å diameter) and slightly wider spherical intersections (~10 Å diameter), which promote decarbonylation, decarboxylation, dehydration, C–O (dealkoxylation), and C–C bond scission reactions, as well as the formation of aromatics via deoxygenation of the initially formed phenolics or via C2=C3= aromatization; these small alkenes can be produced by thermal or catalytic cracking of side alkyl-chains or via dehydration of small intermediate alcohols [43,64,66,68,69]. The relative strength of the Brønsted acid sites of ZSM-5 zeolite is also important as the ZSM-5(40), which has less but stronger acid sites compared to ZSM-5 (11.5) (Table 3, Figure 7, and the related discussion above), exhibited slightly higher reactivity for the conversion of alkoxy-phenols and the production of mono-aromatics, phenols, and PAHS, for both lignins (Figure 9).

When comparing the influence of the type of lignin, i.e., spruce (softwood) vs. birch (hardwood), it can be seen that both microporous ZSM-5 zeolites, i.e., ZSM-5 with an Si/Al ratio of 11.5 and 40, are slightly more active in the conversion of guaiacyl-type compounds originating from spruce lignin compared to the syringyl compounds derived from birch lignin (Figure 9). This leads to a higher increase of alkyl- (non-oxygenated) phenols and PAHs with spruce lignin while the relative concentration of mono-aromatics is similar for both lignins. Furthermore, from the data in Tables S1 and S2, it can also be seen that there is no significant differentiation with regard to the selectivity towards individual mono-aromatic compounds. For both lignins, toluene and 1,3-dimethyl-benzene (m-xylene) were the most abundant aromatics, followed by benzene, 1,2,3-trimethyl-benzene, and mesitylene. Similarly, 1- or 2-methyl-naphthalene and naphthalene were the most abundant PAHs for both lignins while 2- or 3-methyl-phenol and 4-methyl-1,2-benzenediol were the alkyl-phenols with the higher concentration, especially with spruce lignin. Although there are few studies available in the literature that have investigated the fast pyrolysis of different types of lignins, i.e., from different raw biomass (in some cases, mixtures of different wood biomass) or method of isolation [66,105–107], the present work examines specific hardwood (birch) and softwood (spruce) lignins that have been isolated by the same method (organosolv–steam explosion), thus solely elucidating the effect of the botanical origin and excluding the changes induced by the different biomass fractionation methods or the mixing of different biomass sources.

The effect of intracrystal mesoporosity and high external surface (due to nanosized crystals) of ZSM-5 on the composition of the fast pyrolysis oil for the two lignins can be revealed by the data shown in Figure 9, as well as in Tables S1 and S2 (Supplementary Materials). It is clear that the dealkoxylation activity of all three hierarchical ZSM-5 zeolites, i.e., meso-ZSM-5 (45 nm), meso-ZSM-5 (9 nm), and nano-ZSM-5, was substantially higher than that of their corresponding microporous ZSM-5 (11.5) and ZSM-5 (40) zeolites, especially with the two former for which alkoxy-phenols (in the non-catalytic pyrolysis vapors) were almost completely eliminated for both lignins (Figure 9). It should be noted that the two meso-ZSM-5 zeolites have similar acidic characteristics with their microporous counterparts (Table 3, Figure 7), thus attributing their enhanced reactivity mainly to the presence of the intracrystal mesopores and the improved diffusion properties they offer as the average critical diameter of the related alkoxy-phenolics (at least the monomeric compounds produced initially via thermal pyrolysis of lignin) ranges from ca. 7.5 to 10 Å [108]. On the other hand, the nano-ZSM-5 contains fewer Brønsted acid sites, almost half of those of ZSM-5 (40) or meso-ZSM-5 (9.5 nm), as discussed in the previous section, but still exhibits relatively higher reactivity compared to that of microporous ZSM-5 (40) due to its high external surface.

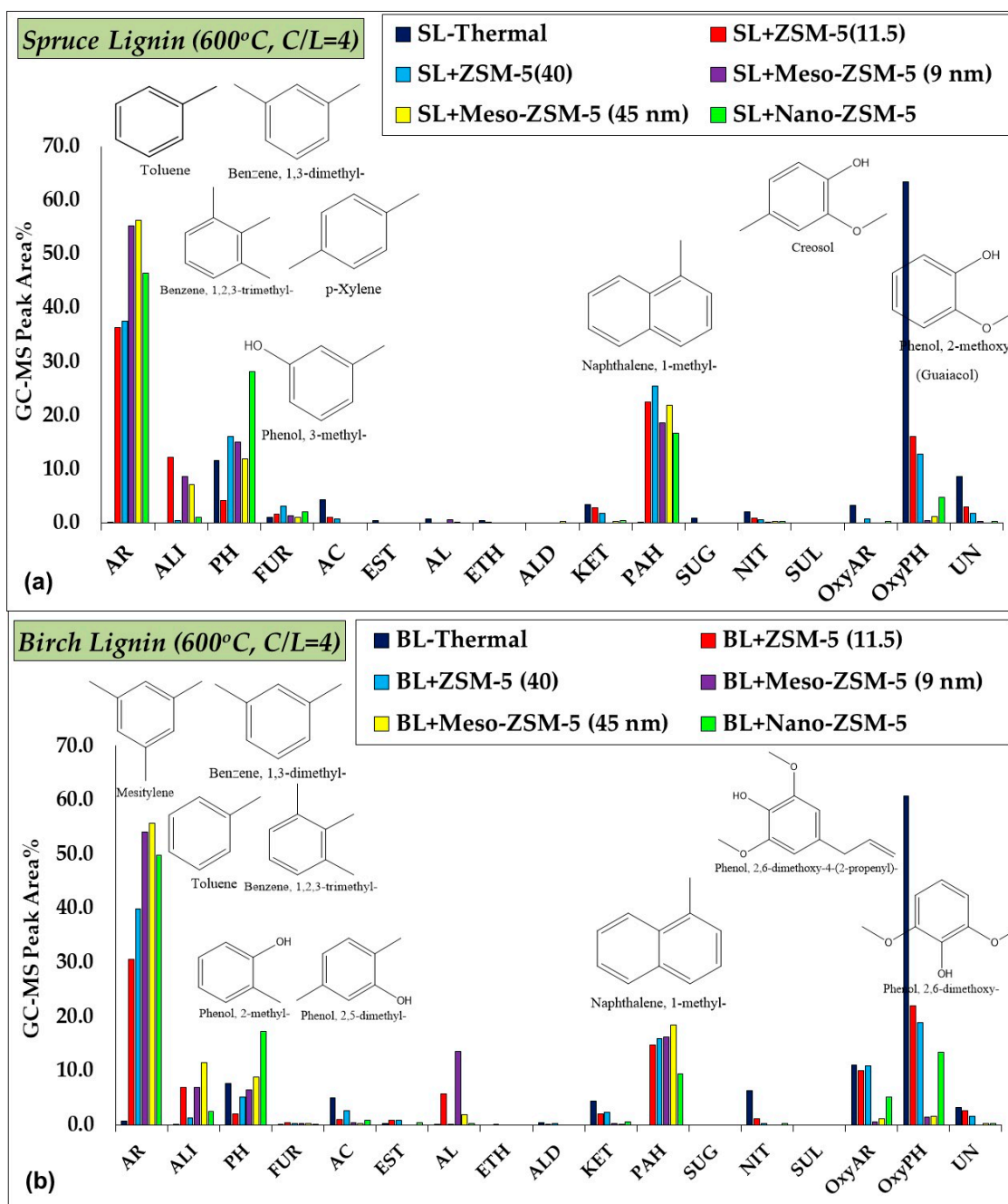


Figure 9. Relative concentration of the various groups of compounds identified in the fast pyrolysis vapors (Py/GC-MS) at 600 °C (catalyst or silica sand to lignin = 4, mass ratio) for: (a) Spruce lignin and (b) birch lignin; most abundant compounds are shown in the graph. Groups of compounds: mono-aromatics (AR), aliphatics (ALI), phenols (PH), furans (FUR), acids (AC), esters (EST), alcohols (AL), ethers (ETH), aldehydes (ALD), ketones (KET), polycyclic aromatic hydrocarbons (PAHs), sugars (SUG) nitrogen compounds (NIT), sulfur compounds (SUL), oxygenated aromatics (OxyAR), oxygenated phenols (OxyPH), and unidentified compounds (UN).

A similar superior behavior of hierarchical ZSM-5 zeolites was also observed in our previous work on the catalytic fast pyrolysis of kraft spruce lignin [43]. However, a substantial difference was observed with those data, i.e., the spruce lignin of the present study (isolated by the organosolv–steam explosion method) offered a much higher concentration of mono-aromatics with the mesoporous zeolites than with the microporous ZSM-5 (Figure 9), compared to the kraft spruce lignin, which, on the

other hand, induced enhanced formation of alkyl- (non-oxygenated) phenols, almost similar to that of aromatics [43]. With the organosolv–steam explosion spruce lignin of the present work, only the nano-ZSM-5 was capable of providing increased selectivity of both mono-aromatics and alkyl-phenols. These directly comparative data reveal the effect of the lignin isolation method on the CFP product selectivity, i.e., aromatics vs. phenols, which may arise from the different structural and compositional characteristics of the lignins. It is also interesting to note that the nitrogen compounds were almost completely eliminated, especially with the hierarchical ZSM-5 zeolites, compared to the non-catalytic pyrolysis vapors for both organosolv lignins (Figure 9 and Tables S1 and S2) while sulfur compounds were absent even in the non-catalytic pyrolysis vapors as both lignins contained only traces of sulfur (Table 1) in contrast to kraft spruce lignin [43].

With regard to the effect of hierarchical zeolites on the individual aromatic and phenolic compounds, as compared to the CFP with the conventional microporous ZSM-5, an increased concentration of the most abundant mono-aromatics was observed, i.e., toluene, 1,3-dimethyl-benzene, 1,2,3-trimethyl-benzene, mesitylene, o-xylene, etc., for both lignins (Tables S1 and S2). In addition, p-xylene was identified in an increased concentration with the meso-ZSM-5 zeolites. Alkyl-phenols, such as 2- or 3-methyl-phenol and dimethyl phenols, were further increased mainly by the nano-ZSM-5 zeolite while PAHs were slightly reduced or increased depending on the lignin origin, as discussed below, with the most representative being the same as those from the conventional ZSM-5s, i.e., naphthalene, 1- or 2-methyl-naphthalene, as well as dimethyl naphthalenes.

When comparing the influence of the type of lignin on the effect of the hierarchical porosity of ZSM-5 zeolite (Figure 9, and Tables S1 and S2), similar trends can be identified in the changes of mono-aromatics and alkyl-phenols for both lignins. In the case of PAHs, a slight variation can be observed, with the two meso-ZSM-5 zeolites inducing less PAHs compared to the microporous ZSM-5 with spruce lignin (in accordance also with the results in [43]) and slightly more with birch lignin. With regard to the individual compounds, no significant influence of the lignin origin can be identified with the exception of slightly increased dimethyl naphthalenes (PAHs) with the birch-derived lignin (Table S1 vs. Table S2).

2.4. Non-Catalytic and Catalytic Fast Pyrolysis of Model Compounds (Py/GC-MS System)

There are several studies available in the literature that have focused on the fast pyrolysis of model lignin compounds, including dimers/oligomers containing β - and α -ether, β -aryl, and other representative bonds in the structure of lignin, as well as in situ spectroscopic investigations that aim to identify the formation of reactive intermediates [109–113]. The reported results and related discussion provide valuable insight but are highly dependent on the type of model compound and experimental pyrolysis/analysis system used, thus suggesting possible reaction mechanisms that cannot be widely adopted. On the other hand, there are many studies that have proposed mechanistic schemes based mainly on the composition of feed (lignin, model molecules) and the obtained final products (aromatics, phenolics, coke, etc.) by utilizing existing knowledge of the acid catalytic function of various zeolites [43,64,66,68,69]. In this work, we studied the fast pyrolysis of two of the most abundant compounds in the fast pyrolysis vapors of spruce and birch lignins (Figures 8 and 9, and Tables S1 and S2), i.e., guaiacol and syringol, which are the most typical model monomer compounds of softwood and hardwood lignins, which also have critical diameters suitable for the pores of conventional and hierarchical ZSM-5 zeolites, as discussed above. Two representative catalysts were selected for this study, i.e., the conventional ZSM-5 (40) and the hierarchical meso-ZSM-5 (9 nm). The distribution of groups of compounds produced in the non-catalytic (silica sand) and catalytic pyrolysis of guaiacol and syringol is presented in Figure 10a,b, respectively. The first important information arises from the relatively higher stability of syringol at 600 °C in the absence of a catalyst (94% of the total GC-MS peak area) compared to guaiacol (52% of the total GC-MS peak area), which was mainly converted to 2-hydroxy-benzaldehyde (19%), alkyl-phenols, such as 2-methyl- and 2-ethyl-phenol (5% each), and catechol (5%). The formation of these three types of compounds has been previously proposed

to occur via homolytic cleavage of the O–CH₃ bond or via O–CH₃ and benzyl ring rearrangement pathways involving radical intermediates [109,114]. On the other hand, the limited conversion of syringol induced the formation of mainly 2-hydroxy-3-methoxy-benzaldehyde, tetra-alkyl phenols, and 2-methoxy-6-methylphenol.

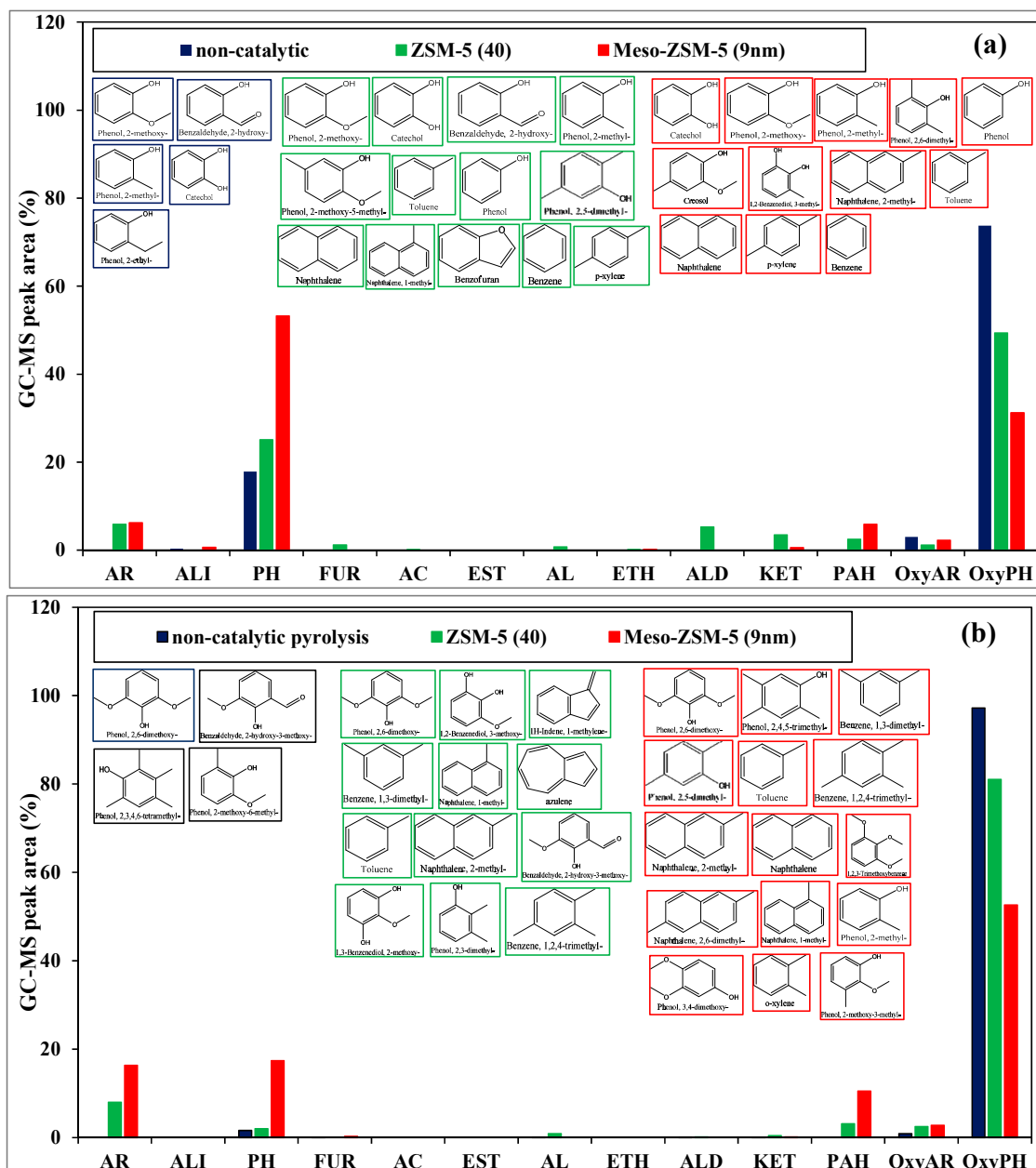


Figure 10. Relative concentration of the various groups of compounds identified in the fast pyrolysis vapors (Py/GC-MS) at 600 °C (catalyst or silica sand to lignin = 4, mass ratio) of (a) guaiacol and (b) syringol, as model compounds existing in the pyrolysis vapors of spruce and birch lignin, respectively; the most abundant compounds are also shown with decreasing concentration from top/left to right.

The catalytic pyrolysis of the model compounds followed the same trend with that of the non-catalytic tests. There is a significant difference in the remaining (not converted) guaiacol (39% of the total GC-MS peak area with ZSM-5 (40) and 19% with meso-ZSM-5 (9 nm)) and syringol (83% with ZSM-5 (40) and 49% with meso-ZSM-5 (9 nm)). The substantial higher conversion of guaiacol with ZSM-5 (40) led to the formation of catechol (13%), 2-hydroxy-benzaldehyde (7.5%), 2-methyl-phenol

(4.4%), 2,5-dimethyl-phenol (3.5%), phenol (2.8%), and toluene (1.5%) and lower percentages of methoxy-methyl-phenols, xylenes, naphthalenes, etc. (Figure 10a). With the mesoporous meso-ZSM-5 (9 nm) zeolite, the conversion of guaiacol was higher, leading to more catechol (20%), 2-methyl-phenol (11%), 2,5-dimethyl-phenol (11%), phenol (5.5%), and toluene (1.9%), as well as more of the rest of the alkyl-phenols, mono-aromatics, and naphthalenes (Figure 10a). It is clear, however, that with both catalysts, the preferred group of products is alkyl-phenols (up to 53%) instead of mono-aromatics (up to 6%). The conversion of syringol with the conventional microporous ZSM-5 (40) was limited, mostly towards mono-aromatics (8%), such as 1-methylene-1H-Indene, dimethyl- and trimethyl-benzenes, and toluene, and very few alkyl-phenols and PAHs (Figure 10b). The meso-ZSM-5 (9 nm) was again more reactive, mainly towards mono-aromatics (16%, as those with ZSM-5 (40), plus *o*-xylene, indenes, and benzene), alkyl-phenols (17%, mainly di- and trimethyl phenols), and PAHs (10%, mainly naphthalene and methyl- or dimethyl naphthalenes) (Figure 10b).

In summary, the main outcomes of the model compounds pyrolysis study were the higher conversion of guaiacol compared to syringol under both non-catalytic and catalytic pyrolysis conditions, the clear benefit of the intracrystal mesoporosity of the ZSM-5 zeolite as was also discussed above for the spruce and birch lignin pyrolysis, and the difference in product selectivity depending on the type of model reactant, i.e., guaiacol exhibiting high selectivity towards alkyl-phenols while syringol led to a more balanced formation of aromatics and phenols. The enhanced reactivity of guaiacol compared to syringol, as well as the higher selectivity towards alkyl-phenols with guaiacol as the reactant, are in accordance with the higher conversion of alkoxy-phenols from spruce lignin and the higher abundance of alkyl-phenols by the use of conventional and mesoporous ZSM-5 zeolites, compared to birch lignin, as discussed above (Figure 9, Tables S1 and S2). On the other hand, both mesoporous ZSM-5 zeolites induced almost complete conversion of the alkoxy-phenols in the thermal pyrolysis vapors of both spruce and lignin (Figure 9) while pure guaiacol and syringol were only partly converted under the same pyrolysis conditions (Figure 10). Furthermore, the clear beneficial effect of meso-ZSM-5 (9 nm) compared to ZSM-5 (40) towards alkyl-phenols from guaiacol (Figure 10a) was also not depicted in the pyrolysis of spruce lignin, where the two catalysts provided a similar abundance of alkyl-phenols (Figure 9a). These data are indicative of the importance and the high reactivity of the initially produced dimers/oligomers in the thermal pyrolysis vapors, which may further react on the catalyst surface before they degrade to more stable monomers (identified in the non-catalytic pyrolysis). It may also be related to the beneficial effect of the acidic surface of micro/mesoporous zeolites and aluminosilicates on the stabilization of the initially formed oligomeric radical intermediates, thus avoiding repolymerization and char/coke formation, and their further conversion via C–C and C–O bond cleavage towards final aromatic and phenolic monomers [68].

2.5. Non-Catalytic and Catalytic Fast Pyrolysis of Spruce and Birch Lignins on the Fixed Bed Downflow Reactor

The non-catalytic and catalytic pyrolysis by two representative zeolites, i.e., microporous ZSM-5 (40) and meso-ZSM-5 (9 nm), of the spruce and birch lignins was also studied on a bench-scale downflow fixed-bed reactor, described previously [43] and in the Supplementary Material, in order to determine the yield of the various products (total liquids, organic bio-oil and water, gases, and solids, i.e., char plus catalytic coke). The yield of total liquids in the non-catalytic experiments were 36.7 (comprising of 31.3 wt.% organic oil and 5.4 wt.% water) and 38.8 wt.% (comprising of 32.8 wt.% organic oil and 5.9 wt.% water) for spruce and birch lignin, respectively (Figure 11a,b and Tables S3 and S4 in Supplementary Material). Accordingly, the non-condensable gases were 15.6 and 13.1 wt.%, and the solids (char) were 42.2 and 42.7 wt.% for the spruce and birch lignin, respectively. In the catalytic pyrolysis with the conventional ZSM-5 (40) zeolite, there was a substantial decrease of the organic fraction of bio-oils (i.e., 19.7 from 31.3 wt.% and 22.6 from 32.8 wt.% for spruce and birch lignin, respectively) with a subsequent increase of water (i.e., 12.3 from 5.4 wt.% and 12.8 from 5.9 wt.% for spruce and birch lignin), leading to a moderate decrease of total liquids (i.e., 32.0 from 36.7 wt.%

and 35.4 from 38.8 wt.% for spruce and birch lignin). The non-condensable gases and solids (char and coke on catalyst) increased by about 3 to 4.5 wt.% for both lignins, with respect to the gases and solids in the non-catalytic experiment. In accordance with the observed higher reactivity of the mesoporous ZSM-5 zeolites compared to the conventional ZSM-5 for converting the alkoxy-phenols, as discussed in the previous section, the above changes in product yields were also slightly enhanced further, by ≤ 4 wt.%, with the use of the mesoporous meso-ZSM-5 (9 nm) zeolite, except in the case of solids in spruce lignin pyrolysis, which were slightly reduced compared to those with ZSM-5 (40) zeolite (Figure 11a,b and Tables S3 and S4). These results are in agreement with our previous study using kraft spruce lignin [43] as well as with other previously reported works with microporous or mesoporous ZSM-5 zeolites on biomass or lignin pyrolysis using a similar experimental set-up consisting of fixed-bed downflow reactors [75,86,106,115,116].

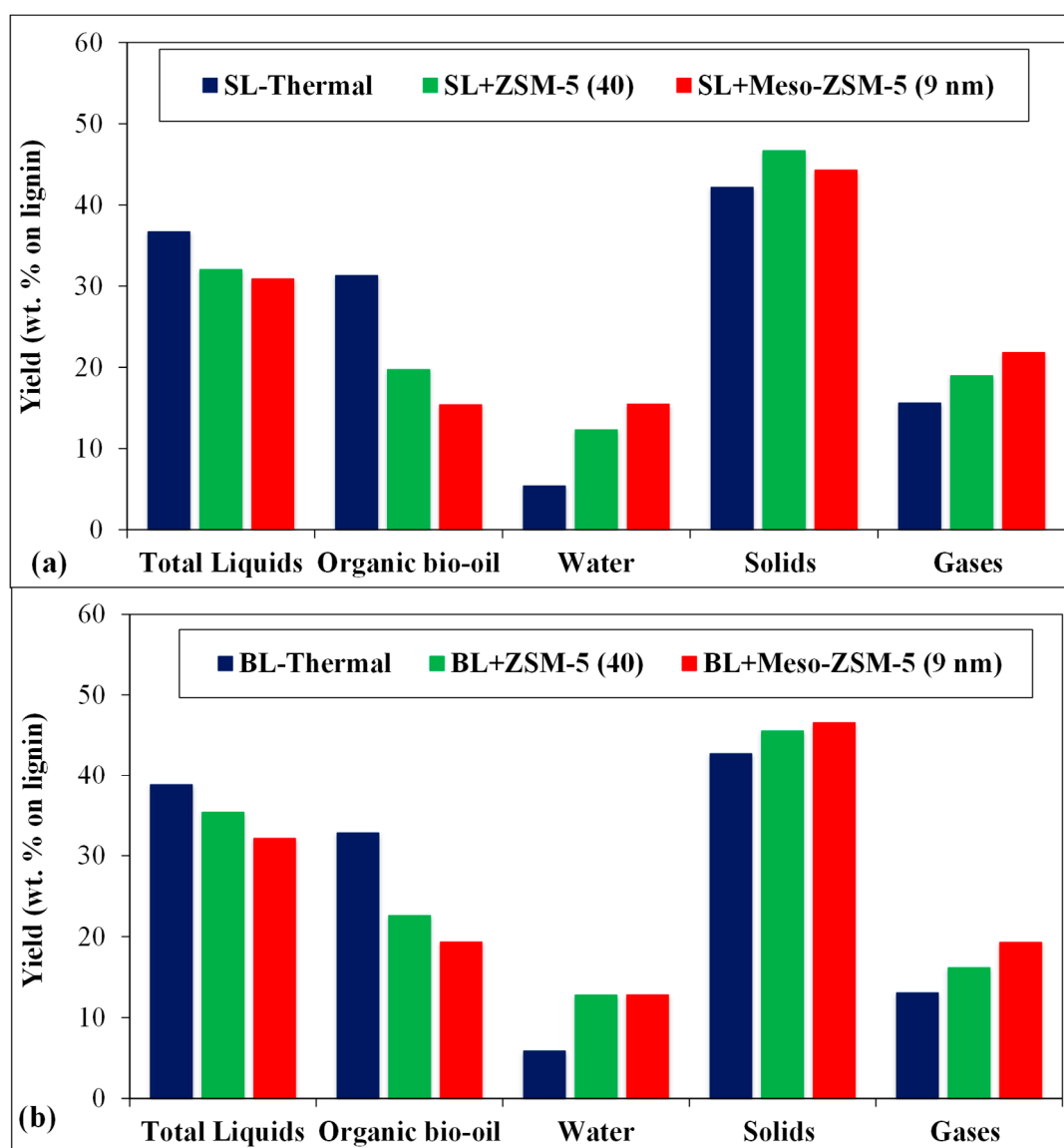


Figure 11. Fixed-bed reactor product yield distribution from the thermal and catalytic fast pyrolysis, at 600 °C (C/L = 1), of: (a) Spruce lignin and (b) birch lignin.

The increased yield of solids in the catalytic pyrolysis experiments is attributed to the formation of coke on the acidic zeolites, mainly via condensation reactions of aromatics, PAHs, or alkyl-phenols, as also shown previously for similar downflow fixed-bed reactors (with separate lignin and catalyst

beds) [43,86,106] or a two consecutive reactors setup [116,117]. These reactor configurations allow for the retrieval of the coked catalyst, which does not come in contact with the original lignin or the thermally produced char, but only with the thermal pyrolysis vapors that react on the catalyst surface. On the other hand, there are many studies available based mainly on pyrolyzer/GC-MS systems, i.e., with tubes [68,71] or buckets [64], which have showed that the use of zeolitic catalysts may induce lower yields of solids (char and coke), and in some cases, a higher yield of bio-oil compared to thermal pyrolysis tests. This was also the case in our previous work on spruce lignin catalytic pyrolysis, where the Py/GC-MS experiments showed reduced solids with both microporous and hierarchical ZSM-5 zeolites compared to the fixed-bed reactor tests [43]. It is thus obvious that different experimental set-ups as well as different conditions, i.e., pyrolysis temperature and catalyst to lignin ratio, may lead to contradictory results with regard to the effect of zeolitic catalysts on the yield of total solids. From the data in Figure 11 and in Tables S3 and S4 (Supplementary Material), it can be seen that both the microporous and mesoporous ZSM-5 zeolite induced a relatively small increase of total solids for both organosolv lignins, with regard to the non-catalytic pyrolysis, and at the same level or slightly lower compared to the use of kraft spruce lignin [43]. It is also interesting to note that despite the enhanced deoxygenation and aromatization activity of meso-ZSM-5 (9 nm) compared to the conventional ZSM-5 (40) zeolite, the intracrystal mesopores did not favor condensation/polymerization reactions towards coke, especially in the case of spruce lignin, where the total solids with the mesoporous ZSM-5 were even reduced compared to the microporous catalyst. The char formed in the non-catalytic experiments and the used catalysts were further studied by TGA/MS (Figure S2, Supplementary Material). The DTG curves of the non-catalytic (thermal) char from spruce and birch pyrolysis exhibited well-defined peaks with maxima at 528 and 541 °C, respectively, thus indicating a similar structure/composition. The DTG curve of the used catalysts from spruce lignin CFP exhibited a similar peak as the thermal char and an additional broad shoulder exceeding up to ca. 670 °C, which is probably attributed to the more condensed nature of reaction/aromatic coke formed on the catalysts (further dedicated studies are needed to identify the exact structure of char vs. coke). A similar DTG profile can be seen for the used catalysts from birch lignin CFP (Figure S2, Supplementary Material). It is also evident that some nitrogen was trapped in both char and coke while sulfur is negligible in all cases, in accordance with the elemental analysis data of the parent lignins (Table 1).

The changes induced in the composition of the catalytic bio-oils compared to the non-catalytic ones were similar to those described above for the Py/GC-MS experiments (data not shown for brevity). The composition analysis of the non-condensable gases is shown in Figure 12. The thermal pyrolysis gases consisted mainly of CO, CO₂ as well as some methane, typical for biomass and lignin fast pyrolysis. The use of ZSM-5 zeolite catalysts induced higher CO and CO₂ yields due to enhanced decarbonylation and decarboxylation reactions, which are the main routes of deoxygenation with ZSM-5 zeolites, in addition to dehydration (water production) [43,116]. In addition, ethylene and propylene were formed, which indicates the promotion of cracking and dealkylation reactions by ZSM-5. The higher yield of these gases with meso-ZSM-5 (9 nm) zeolite compared to microporous ZSM-5 is an indication of its enhanced cracking activity, in addition to the higher deoxygenation activity, of primary alkylated alkoxy-phenols. As discussed above and in accordance with the suggested reaction mechanisms in the literature, these small alkenes are precursors of mono-aromatics in lignin CFP via the known aromatization activity of ZSM-5 [43,66].

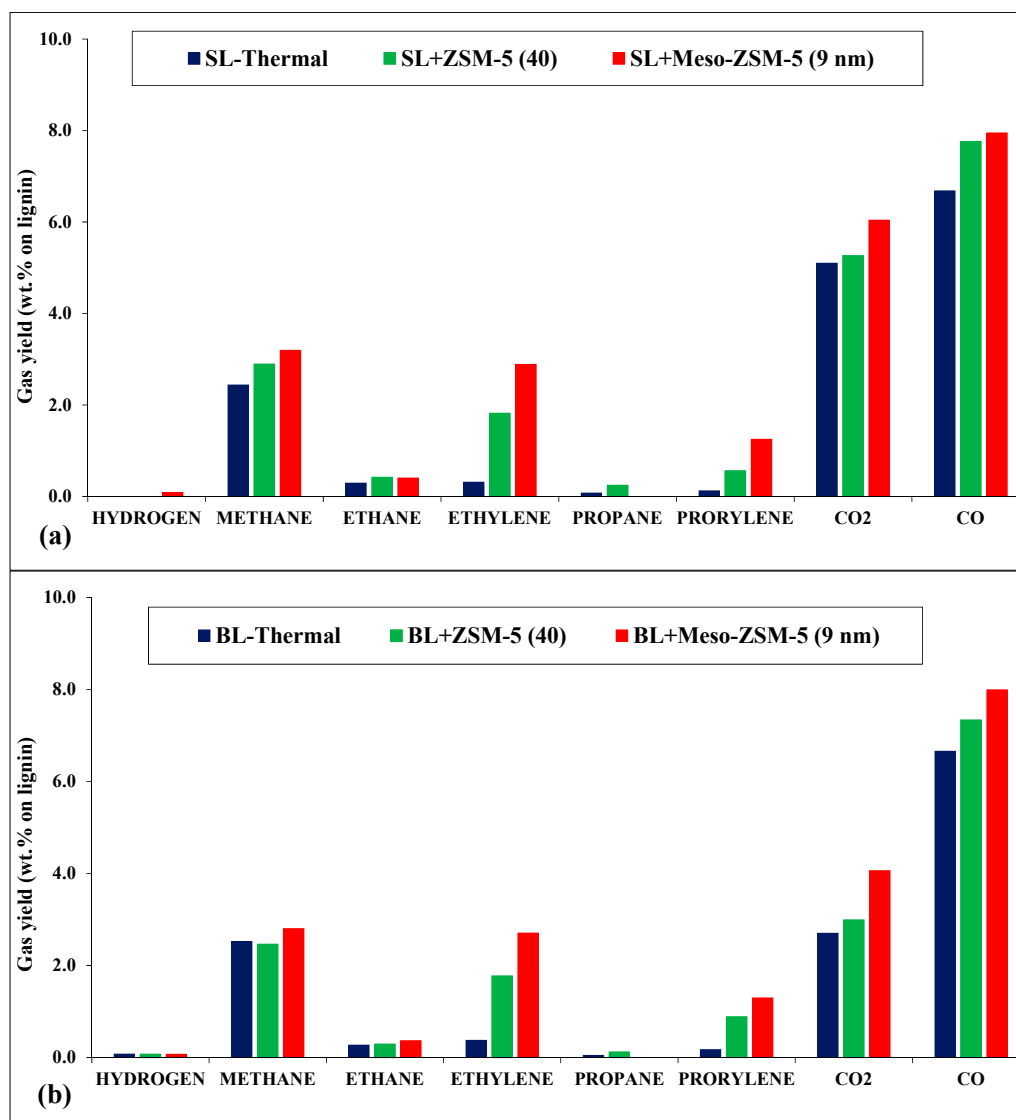


Figure 12. Composition of non-condensable gases derived from the thermal and catalytic fast pyrolysis on the fixed bed reactor at 600 °C (C/L = 1), of (a) Spruce Lignin and (b) Birch Lignin.

3. Materials and Methods

3.1. Production and Characterization of Organosolv Lignin

Lignin production was performed by a hybrid steam explosion—organosolv pretreatment process which combines the benefits of the two individual methods, as recently reported for the pretreatment of typical softwood (spruce) and hardwood (birch) biomass [23,34,35]. In short, 200 g of either spruce or birch biomass were mixed with 400 g of ethanol and were manually introduced in a hybrid reactor. After closing the reactor, the rest of the ethanol required to attain the desired ethanol content (52% or 60% v/v for spruce and birch, respectively) was loaded by using an external pump. The reactor was heated at 200 °C with external electrical heating elements and steam. The pretreatment duration was 30 and 15 min for spruce and birch, respectively [34,35]. At the end of the cooking time, the reactor was rapidly discharged by opening the discharge valve, causing the explosion of the pretreated slurry through the cyclone into the collection vessel. The slurry was then collected, and the solids were separated from the liquor by vacuum filtration. Finally, to allow lignin separation from the liquor, the ethanol was recovered in a rotary evaporator, effectively reducing the lignin solubility. Lignin was then collected by centrifugation (14,000 rpm, at 4 °C for 15 min), followed by its drying at ambient

temperature and storage at room temperature. Prior to any characterization, the lignin samples were further dried at 80 °C for 6 h under vacuum.

The elemental analysis of dried lignin samples was carried out on a EuroEA 3000 C/H/N/S Analyzer (EuroVector, Pavia, PV, Italy); the oxygen content was calculated by the difference. The thermogravimetric analysis (TGA) experiments were conducted on a NETZSCH STA 449 F5 Jupiter analyzer (NETZSCH, Selb, Germany), using dried lignin samples. The samples were heated from room temperature to 850 °C, with a heating rate of 10 °C/min, using N₂ as the carrier gas (purity >99.999 vol.%) at a flow rate of 50 mL/min.

The molecular weight distribution and the average molecular weight of the lignin samples were determined by gel permeation chromatography (GPC) as previously described [22]. In a typical measurement, ~5 mg of lignin were suspended in 1 mL of glacial acetic acid/acetyl bromide (9:1 v/v; Sigma Aldrich, St. Louis, MO, USA) for ~2 h [85]. Then, the organic reagents were removed in a vacuum evaporator and the remaining solids were washed twice by dissolving them in 1 mL of THF (tetrahydrofuran; VWR Chemicals, Radnor, PA, USA) followed by evaporation of THF. Finally, the sample was dissolved in 1 mL of THF and used for analysis. Analysis took place in a PerkinElmer Flexar (Watham, MA, USA) HPLC apparatus equipped with a UV detector (set at 280 nm). For the analysis, the Styragel HR 4E (Waters; Miford, MA, USA) chromatographic column was used, which was kept at 40 °C and the THF mobile phase with a flowrate of 0.6 mL/min. Calibration of GPC was carried out with standard polystyrene samples (Sigma Aldrich).

The 2D HSQC NMR spectra were obtained on a Varian (Agilent Technologies, California, CA, USA) 500 MHz DD2 spectrometer. In total, 100 mg of the lignin samples were dissolved in 0.45 mL of DMSO-d₆ (dimethylsulfoxide-d₆), 99.8% (Deutero GmbH, Kastellaun, Germany) and stirred overnight before the analysis. The chemical shifts were referenced to the solvent signal (2.500/39.520 ppm). The relaxation delay was set to 5 s, which has been found to be a sufficient time for full relaxation of the signals [118]. The spectral widths were from 13 to −1 ppm and from 160 to 0 ppm for the ¹H and ¹³C dimensions, respectively. The number of transients was 16 or 32, and 256 time increments were recorded in the ¹³C dimension. The spectra were processed using MestReNova software. Prior to Fourier transformation, FID (free induction decay) signals were apodized with a $\pi/2$ sine squared bell function in both dimensions. The relative abundance of each type of aromatic unit, each type of linkage, and each type of end-group was calculated by integration of the respective correlation peaks, as described in more detail in the Supplementary Material. The areas of the C _{α} -H _{α} correlation peaks of A, B, or C types of inter-unit linkages were used for the calculation of their relative abundance.

3.2. Catalysts Preparation and Characterization

Two conventional microporous ZSM-5 zeolites with different Si/Al ratios, two mesoporous ZSM-5 with different mesopore sizes, and one nano-sized ZSM-5 were tested in lignin catalytic fast pyrolysis (CFP). The microporous zeolites, CBV 2314 (Si/Al = 11.5) and CBV 8014 (Si/Al = 40), were provided by Zeolyst in their ammonium form and were converted to the proton form via calcination in air at 500 °C for 3 h; they were denoted as ZSM-5 (11.5) and ZSM-5 (40), respectively. A mesoporous ZSM-5 sample, denoted as meso-ZSM-5 (9 nm), was prepared by mild alkaline treatment of H-CBV 8014 (Si/Al = 40) zeolite with 0.2 M NaOH aq. solution at 65 °C for 30 min under stirring, followed by treatment with 0.1 N HCl aq. solution at 65 °C for 6 h under stirring. A second mesoporous sample, denoted as meso-ZSM-5 (45 nm), was prepared from H-CBV 2314 (Si/Al = 11.5) by the same method as for meso-ZSM-5 (9 nm), except that a 1 M NaOH aq. solution was used in this case (the detailed procedure is described in the Supplementary Material). The nanosized zeolite (denoted as nano-ZSM-5) was synthesized based on typical templated hydrothermal methods applied for ZSM-5 zeolites, using tetraethylorthosilicate (TEOS, 98%, Sigma-Aldrich, St. Louis, MO, USA) and aluminum-tri-sec-butoxide (97%, Sigma-Aldrich) as Si and Al sources, and 1 M tetrapropylammonium hydroxide (TPAOH, Sigma-Aldrich) solution as the structure-directing agent for MFI-type zeolite. In short, TEOS and Al-tri-sec-butoxide were initially mixed under stirring followed by the addition of

TPAOH solution (mixture molar ratio: 1 SiO₂:0.01 Al₂O₃:0.37 TPAOH:16.4 H₂O) and further stirring for 1 h at room temperature. The formed suspension was further hydrothermally aged at 100 °C for 4 days, followed by filtration, thorough washing, drying (100 °C overnight), and calcination (600 °C, 6 h, in air). Prior to lignin CFP tests on the fixed-bed reactor, all the zeolite samples were pelletized, crushed, and sieved to a particle size of 180 to 500 µm.

The chemical composition of the zeolites was determined by inductive coupled plasma-atomic emission spectroscopy (ICP-AES) using a Plasma 400 (Perkin Elmer; Waltham, Massachusetts, MA, USA) spectrometer, equipped with a Cetac6000AT+ ultrasonic nebulizer.

Nitrogen adsorption/desorption measurements at −196 °C were performed on an Automatic Volumetric Sorption Analyzer (Autosorb-1MP, Quantachrome Instruments, Boynton Beach, FL, USA). The samples were previously outgassed at 350 °C for 16 h under 5×10^{-9} Torr vacuum. The BET area (i.e., total surface area) of the catalysts was determined by the multi-point BET method, the mesopore width distribution by the BJH analysis of the adsorption data, and the micropore volume and area by the t-plot method.

Powder X-ray diffraction (XRD) was applied for the determination of the crystallinity of zeolites using a Rigaku Rotaflex 200B diffractometer (RIGAKU Co., Ltd., Tokyo, Japan) equipped with Cu Ka X-ray radiation and a curved crystal graphite monochromator operating at 45 kV and 100 mA; counts were accumulated in the range of 5 to 75° 2θ every 0.02° with a counting time of 2 sec per step.

Electron microscopy (TEM-HRTEM) experiments were carried out on a JEOL 2011 (JEOL Ltd., Tokyo, Japan) high-resolution transmission electron microscope operating at 200 kV, with a point resolution of 0.23 nm and Cs = 1.0 mm. Samples were prepared by grinding the catalyst in high-purity ethanol using an agate pestle and mortar. A drop of the suspension was subsequently deposited onto a lacey carbon-film supported on a Cu grid and allowed to evaporate under ambient conditions.

The determination of the amount and relative strength of Brønsted and Lewis acid sites of the catalysts was performed by Fourier transform-infrared (FT-IR) spectroscopy combined with in situ adsorption of pyridine on a Nicolet 5700 FTIR spectrometer (Thermo Fisher Scientific, Waltham, Massachusetts, MA, USA) with resolution 4 cm^{−1}, using the OMNIC software (Thermo Fisher Scientific, Waltham, Massachusetts, MA, USA) and a specially designed heated, high-vacuum infrared (IR) cell with CaF₂ windows, as described in detail in the Supplementary Material and in our previous work [43].

3.3. Fast Pyrolysis Experiments Using the Py/GC-MS System

Thermal (non-catalytic) and catalytic fast pyrolysis experiments of the spruce- and birch-derived lignins were performed on a Multi-Shot Micro-Pyrolyzer (EGA/PY-3030D, Frontier Laboratories, Fukushima, Japan) connected to a gas chromatographer-mass spectrometer system (GC-MS-QP2010, Shimadzu Corp., Kyoto, Japan). In brief, a mixture of 1 mg of lignin (dried at 80 °C, under vacuum for 6 h) and 4 mg of silica sand (as the inert heat carrier material) or catalyst were loaded in a stainless-steel cup, which was instantaneously dropped in the hot reactor/furnace and pyrolysis was conducted at the preset temperature of 600 °C for 12 s. Identification of mass spectra peaks was achieved online by the use of the scientific library NIST11s (Scientific Instrument Services, Ringoes, NJ, USA). The derived compounds were classified and categorized under the following 16 groups and families: Mono-aromatics (AR); aliphatics (ALI); phenols (PH), including substituted phenols with functional groups, such as aldehydes and ketones; acids (AC); esters (EST); alcohols (AL); ethers (ETH); aldehydes (ALD); ketones (KET); polycyclic aromatic hydrocarbons (PAHs); sugars (SUG); nitrogen compounds (NIT); sulfur compounds (SUL); oxygenated aromatics (OxyAR); oxygenated phenols (OxyPH), including substituted oxy-phenols with functional groups and unidentified compounds (UN). Model compound (i.e., guaiacol and syringol) pyrolysis experiments were also conducted following the same protocol as for the lignin pyrolysis tests. At least three experiments were performed for each lignin or model compound/catalyst sample and the reported data represent their mean values with

standard deviation, in all cases, being below 10%. A detailed description of the experimental set-up and procedure is provided in the Supplementary Material (Figure S3).

3.4. Fast Pyrolysis Experiments Using a Downflow Fixed-Bed Reactor

Fast pyrolysis tests were also carried out on a bench-scale, downflow, fixed-bed tubular reactor made of stainless-steel 316 and heated by a 3-zone furnace. A specially designed piston system was used to introduce lignin into the reactor. The amount of lignin (dried at 80 °C under vacuum for 6 h) used in all experiments was 0.4 g and the amount of silica sand (thermal pyrolysis experiments, non-catalytic) or catalyst (in the catalytic experiments) was also 0.4 g. In a typical experiment, the solid lignin was inserted from the top of the reactor and was pushed down instantaneously with the aid of the piston in the hot reactor zone, where it was vaporized at 600 °C. The pyrolysis vapors produced were driven downwards through the catalyst bed with the aid of a constant N₂ flow (100 cm³/min), for 20 min. The product vapors were condensed in pre-weighted spiral glass receivers that were immersed in a cooling bath (−20 °C). Bio-oil was collected with 1 mL of methanol and was analyzed by GC-MS (GC-MS-QP2010, Shimadzu). For the identification of the relative abundance of the produced compounds in bio-oil, the NIST11s mass spectral library was used and the derived compounds were classified and categorized in the 16 groups and families, as in the case of the Py/GC-MS experiments. The water content of bio-oil was determined by Karl–Fischer (Metrohm AG, Herisau, Switzerland) titration (ASTM E203-08) while elemental analysis (C/H/N/S) of the organic fraction of the bio-oil was determined by a Euro EA 2000 C/H/N/S Elemental Analyzer; oxygen was determined by the difference.

The solids products, which comprised of char in the non-catalytic pyrolysis experiments and char plus coke-on-catalyst in the catalytic pyrolysis experiments, were determined by direct weighting. An indirect estimation of the coke formed on the catalyst, as wt.% on initial lignin, was performed by subtracting the measured char content of the non-catalytic experiment from the char + coke content of the catalytic experiments (char formation is not affected by the presence of the catalysts, as lignin and catalysts do not come in contact; see a detailed description of the experimental unit and procedure in the Supplementary Materials, Figure S4). Furthermore, the decomposition profile of the collected char and coke (on the spent catalysts) was studied by thermogravimetric analysis (TG-DSC, NETZSCH STA 449 F5 Jupiter, NETZSCH, 95100 Selb Germany) coupled with an on-line mass spectrometer (QMS 403 Aeolus Quadro, NETZSCH, 95100 Selb Germany), using dry air as the carrier gas, at a flow rate of 50 mL/min. The samples were heated from room temperature to 950 °C at a heating rate of 10 °C/min.

The non-condensable gases (NGCs) in the pyrolysis experiments were measured by the liquid displacement method and were analyzed by GC equipped with TCD and FID (HP5890 Series II) (Agilent Technologies, Santa Clara, CA, USA). More details on the experimental set-up and analytic procedures are provided in the Supplementary Material (Figure S4). The standard deviation of the product yield values reported, at all cases, is below 5%.

4. Conclusions

It was shown that the thermal (non-catalytic) fast pyrolysis oil of spruce and birch lignins, which was isolated by a hybrid organosolv–steam explosion method, has a similar composition profile with the parent lignin in terms of phenylpropane units. In the case of spruce, the bio-oil contained mainly alkoxy-phenols, with a single methoxy-group originating from the abundant coniferyl (guaiacyl, G-units) alcohol units in the structure of softwood, while in the case of birch, an S/G ratio of 70/30 (S for syringol-type compounds originating from sinapyl alcohol units) was identified in the bio-oil, similar to that determined by 2D HSQC NMR in the parent lignin (S/G = 77/22).

In the catalytic fast pyrolysis (Py/GC-MS system, at 600 °C), the conventional microporous ZSM-5 zeolites converted the alkoxy-phenols to BTX mono-aromatics, alkyl-phenols, and PAHs (mainly naphthalenes). The ZSM-5 catalysts were slightly more reactive in the conversion of guaiacyl-type alkoxy-phenols compared to syringyl compounds, which were initially formed via thermal pyrolysis of spruce and birch lignin, respectively, leading to a larger increase of alkyl-phenols and PAHs

with spruce lignin, while the relative abundance of mono-aromatics was similar for both lignins. However, the different origin and composition of lignins had no significant effect on the selectivity towards individual mono-aromatic compounds, and for both lignins, toluene and 1,3-dimethyl-benzene (m-xylene) were the most abundant mono-aromatics (followed by benzene, 1,2,3-trimethyl-benzene, and mesitylene), 1- or 2-methyl-naphthalene and naphthalene were the most abundant PAHs, and 2- or 3-methyl-phenol and 4-methyl-1,2-benzenediol were the alkyl-phenols with the higher concentration, especially with spruce lignin. No sulfur compounds were identified in the bio-oil, in accordance with the elemental analysis of the parent lignins, while the nitrogen compounds found in the thermal bio-oil were almost completely eliminated by the use of the zeolitic catalysts.

The hierarchical ZSM-5 zeolites tested, i.e., meso-ZSM-5 (45 nm) and nano-ZSM-5 (9 nm) with intracrystal mesoporosity and nano-ZSM-5 with a high external surface, exhibited substantially higher dealkoxylation activity compared to the conventional microporous ZSM-5 zeolites, owing to their enhanced diffusion characteristics and the higher available external surface for reaction. On the other hand, the hierarchical zeolites did not induce any significant changes on the selectivity of the individual aromatic and phenolic compounds, as compared to the CFP with the conventional ZSM-5, and further increased the concentration of the most abundant mono-aromatics for both lignins. With regard to the type of lignin, no significant influence was observed on the performance of the hierarchical zeolites, with the exception of slightly increased dimethyl naphthalenes (PAHs) with the birch-derived lignin. However, a substantial difference was observed between the organosolv spruce lignin of the present study and kraft spruce lignin (previous study, [43]), with the former being significantly more selective towards mono-aromatics with the mesoporous ZSM-5 zeolites.

The fast pyrolysis experiments with two representative model compounds, i.e., guaiacol and syringol, revealed a higher conversion of guaiacol compared to syringol under both non-catalytic and catalytic pyrolysis conditions, the clear benefit of the intracrystal mesoporosity of the ZSM-5 zeolite, and the difference in product selectivity depending on the type of model reactant, i.e., guaiacol exhibited high selectivity towards alkyl-phenols while syringol led to a more balanced formation of aromatics and phenols. Although these observations are in line and may support the fast pyrolysis results obtained for spruce and birch lignins, several other differences in reactivity and product selectivity indicated the important effect of the initially formed oligomeric radical intermediates (dimers/oligomers) in thermal pyrolysis vapors, which may further react on the catalyst surface before they degrade to more stable monomers, such as guaiacol and syringol.

The downflow fixed-bed reactor experiments showed the typical effect of conventional ZSM-5 zeolites on the product yields compared to the non-catalytic pyrolysis of lignin, such as the substantial decrease of the organic fraction of bio-oil and the increase of water production, accompanied by a relatively small increase of non-condensable gases and of the already high total solids, due to additional coke formation on the catalysts. The observed changes in product yields were slightly increased further by the use of the mesoporous ZSM-5 zeolite. TGA/MS analysis of the non-catalytic (thermal) char and the separately used catalysts indicated the additional formation of more condensed coke/char on the zeolitic catalysts compared to the thermal char. Analysis of the non-condensable gases showed the enhanced production of ethylene and propylene with the ZSM-5 zeolites, in addition to the typical lignin pyrolysis gases (CO, CO₂, and methane). The production of light alkenes was more pronounced with the mesoporous ZSM-5 zeolite, thus supporting an enhanced aromatization mechanism on these zeolites and justifying the observed high selectivity towards BTX mono-aromatics for both spruce and birch lignins.

Supplementary Materials: The following are available online at <http://www.mdpi.com/2073-4344/9/11/935/s1>, Figure S1: Representative TEM images of the commercial microporous zeolite ZSM-5 (40), Figure S2: DTG curves (a) of char from spruce and birch lignin non-catalytic pyrolysis at 600 °C, (b) of coked Meso-ZSM-5 (9 nm) zeolite from catalytic fast pyrolysis of spruce lignin, and (c), (b) of coked Meso-ZSM-5 (9nm) zeolite from catalytic fast pyrolysis of birch lignin. The on-line MS signals of NO_x (m/e 46) and SO_x (m/e 64) are also shown in order to identify any S and N admixtures in char/coke; the thermal analyses were performed under oxidative (air) atmosphere, Figure S3: Schematic representation of Py/GC-MS system, Figure S4: Schematic representation

of bench-scale downflow fixed bed reactor for lignin fast pyrolysis, Table S1: Composition of bio-oil derived from non-catalytic and catalytic fast pyrolysis of Spruce lignin in the Py/GC-MS system (GC-MS peak area, %). The catalytic results refer to experiments at 600 °C with catalyst to lignin (C/L) ratio of 4, Table S2: Composition of bio-oil derived from non-catalytic and catalytic fast pyrolysis of Birch lignin in the Py/GC-MS system (GC-MS peak area, %). The catalytic results refer to experiments at 600 °C with catalyst to lignin (C/L) ratio of 4, Table S3: Product yields (wt.% on lignin) and bio-oil composition for the thermal and catalytic pyrolysis of spruce lignin on the fixed-bed reactor at 600 °C (Cat/Lignin = 1), Table S4: Product yields (wt.% on lignin) and bio-oil composition for the thermal and catalytic pyrolysis of birch lignin on fixed-bed reactor at 600 °C (Cat/Lignin = 1),

Author Contributions: Conceptualization, K.T., P.L., L.M., and P.C.; methodology, P.L. and L.M.; formal analysis and investigation, I.C., P.L., A.F., E.P., and L.M.; resources, K.T., U.R. and P.C.; writing—original draft preparation, I.C., P.L., A.F. and L.M.; writing—review and editing, I.C., L.M., P.C., and K.T.; supervision, I.C., P.L. and L.M.; project administration, I.C., P.L. and L.M.; funding acquisition, K.T., U.R. and P.C.

Funding: L.M., U.R. and P.C. would like to thank Bio4Energy, a strategic research environment appointed by the Swedish government for providing funding to the current research work.

Acknowledgments: We thank Sveaskog, Sweden, for providing the birch and spruce chips that were used in this study. The contribution of COST Action LignoCOST (CA17128), supported by COST (European Cooperation in Science and Technology), in promoting interaction, exchange of knowledge and collaborations in the field of lignin valorization is gratefully acknowledged.

Conflicts of Interest: The authors declare no conflict of interest.

References

1. Huber, G.W.; Iborra, S.; Corma, A. Synthesis of Transportation Fuels from Biomass: Chemistry, Catalysts, and Engineering. *Chem. Rev.* **2006**, *106*, 4044–4098. [[CrossRef](#)]
2. Triantafyllidis, K.S.; Lappas, A.A.; Stöcker, M. *The Role of Catalysis for the Sustainable Production of Bio-Fuels and Bio-Chemicals*; Elsevier: Amsterdam, The Netherlands, 2013.
3. Isikgor, F.H.; Becer, C.R. Lignocellulosic biomass: A sustainable platform for the production of bio-based chemicals and polymers. *Polym. Chem.* **2015**, *6*, 4497–4559. [[CrossRef](#)]
4. Luque, R.; Len, C.; Triantafyllidis, K. Editorial: Nano-(Bio)Catalysis in Lignocellulosic Biomass Valorization. *Front. Chem.* **2018**, *6*, 577. [[CrossRef](#)] [[PubMed](#)]
5. Mosier, N.; Wyman, C.; Dale, B.; Elander, R.; Lee, Y.; Holtzapple, M.; Ladisch, M. Features of promising technologies for pretreatment of lignocellulosic biomass. *Bioresour. Technol.* **2005**, *96*, 673–686. [[CrossRef](#)] [[PubMed](#)]
6. Petridis, L.; Smith, J.C. Molecular-level driving forces in lignocellulosic biomass deconstruction for bioenergy. *Nat. Rev. Chem.* **2018**, *2*, 382–389. [[CrossRef](#)]
7. Krasznai, D.J.; Champagne Hartley, R.; Roy, H.M.; Champagne, P.; Cunningham, M.F. Compositional analysis of lignocellulosic biomass: Conventional methodologies and future outlook. *Crit. Rev. Biotechnol.* **2018**, *38*, 199–217. [[CrossRef](#)]
8. Zakzeski, J.; Bruijninx, P.C.A.; Jongerius, A.L.; Weckhuysen, B.M. The Catalytic Valorization of Lignin for the Production of Renewable Chemicals. *Chem. Rev.* **2010**, *110*, 3552–3599. [[CrossRef](#)]
9. Azadi, P.; Inderwildi, O.R.; Farnood, R.; King, D.A. Liquid fuels, hydrogen and chemicals from lignin: A critical review. *Renew. Sustain. Energy Rev.* **2013**, *21*, 506–523. [[CrossRef](#)]
10. Li, C.; Zhao, X.; Wang, A.; Huber, G.W.; Zhang, T. Catalytic Transformation of Lignin for the Production of Chemicals and Fuels. *Chem. Rev.* **2015**, *115*, 11559–11624. [[CrossRef](#)]
11. Rinaldi, R.; Jastrzebski, R.; Clough, M.T.; Ralph, J.; Kennema, M.; Bruijninx, P.C.; Weckhuysen, B.M. Paving the way for lignin valorisation: recent advances in bioengineering, biorefining and catalysis. *Angew. Chem. Int. Ed.* **2016**, *55*, 8164–8215. [[CrossRef](#)]
12. Zhu, G.; Qiu, X.; Zhao, Y.; Qian, Y.; Pang, Y.; Ouyang, X. Depolymerization of lignin by microwave-assisted methylation of benzylic alcohols. *Bioresour. Technol.* **2016**, *218*, 718–722. [[CrossRef](#)] [[PubMed](#)]
13. Watanabe, M.; Kanaguri, Y.; Smith, R.L. Hydrothermal separation of lignin from bark of Japanese cedar. *J. Supercrit. Fluids* **2018**, *133*, 696–703. [[CrossRef](#)]
14. Cao, L.; Yu, I.K.; Liu, Y.; Ruan, X.; Tsang, D.C.; Hunt, A.J.; Ok, Y.S.; Song, H.; Zhang, S. Lignin valorization for the production of renewable chemicals: State-of-the-art review and future prospects. *Bioresour. Technol.* **2018**, *269*, 465–475. [[CrossRef](#)] [[PubMed](#)]

15. Chakar, F.S.; Ragauskas, A.J. Review of current and future softwood kraft lignin process chemistry. *Ind. Crop. Prod.* **2004**, *20*, 131–141. [[CrossRef](#)]
16. Dhyani, V.; Bhaskar, T. A comprehensive review on the pyrolysis of lignocellulosic biomass. *Renew. Energy* **2018**, *129*, 695–716. [[CrossRef](#)]
17. Lora, J.H.; Glasser, W.G. Recent Industrial Applications of Lignin: A Sustainable Alternative to Nonrenewable Materials. *J. Polym. Environ.* **2002**, *10*, 39–48. [[CrossRef](#)]
18. Carrott, P.J.M.; Carrott, M.R. Lignin—from natural adsorbent to activated carbon: A review. *Bioresour. Technol.* **2007**, *98*, 2301–2312.
19. Da Silva, E.B.; Žabková, M.; Araujo, J.; Cateto, C.; Barreiro, M.; Belgacem, M.N.; Rodrigues, A.; Barreiro, F.; Rodrigues, A. An integrated process to produce vanillin and lignin-based polyurethanes from Kraft lignin. *Chem. Eng. Res. Des.* **2009**, *87*, 1276–1292. [[CrossRef](#)]
20. Strassberger, Z.; Tanase, S.; Rothenberg, G. The pros and cons of lignin valorisation in an integrated biorefinery. *RSC Adv.* **2014**, *4*, 25310–25318. [[CrossRef](#)]
21. Patil, S.; Sen, S.; Argyropoulos, D.S. Thermal properties of lignin in copolymers, blends, and composites: A review. *Green Chem.* **2015**, *17*, 4862–4887.
22. Mu, L.; Wu, J.; Matsakas, L.; Chen, M.; Rova, U.; Christakopoulos, P.; Zhu, J.; Shi, Y. Two important factors of selecting lignin as efficient lubricating additives in poly (ethylene glycol): Hydrogen bond and molecular weight. *Int. J. Boil. Macromol.* **2019**, *129*, 564–570. [[CrossRef](#)] [[PubMed](#)]
23. Nitsos, C.; Matsakas, L.; Triantafyllidis, K.; Rova, U.; Christakopoulos, P. Investigation of different pretreatment methods of Mediterranean-type ecosystem agricultural residues: Characterisation of pretreatment products, high-solids enzymatic hydrolysis and bioethanol production. *Biofuels* **2018**, *9*, 545–558. [[CrossRef](#)]
24. Nitsos, C.K.; Matis, K.A.; Triantafyllidis, K.S. Optimization of Hydrothermal Pretreatment of Lignocellulosic Biomass in the Bioethanol Production Process. *ChemSusChem* **2013**, *6*, 110–122. [[CrossRef](#)] [[PubMed](#)]
25. Nitsos, C.K.; Choli-Papadopoulou, T.; Matis, K.A.; Triantafyllidis, K.S. Optimization of Hydrothermal Pretreatment of Hardwood and Softwood Lignocellulosic Residues for Selective Hemicellulose Recovery and Improved Cellulose Enzymatic Hydrolysis. *ACS Sustain. Chem. Eng.* **2016**, *4*, 4529–4544. [[CrossRef](#)]
26. Nitsos, C.K.; Lazaridis, P.A.; Mach-Aigner, A.; Matis, K.A.; Triantafyllidis, K.S. Enhancing Lignocellulosic Biomass Hydrolysis by Hydrothermal Pretreatment, Extraction of Surface Lignin, Wet Milling and Production of Cellulolytic Enzymes. *ChemSusChem* **2019**, *12*, 1179–1195. [[CrossRef](#)]
27. Jacquet, N.; Maniet, G.; Vanderghem, C.; Delvigne, F.; Richel, A. Application of Steam Explosion as Pretreatment on Lignocellulosic Material: A Review. *Ind. Eng. Chem. Res.* **2015**, *54*, 2593–2598. [[CrossRef](#)]
28. Pielhop, T.; Amgarten, J.; Von Rohr, P.R.; Studer, M.H. Steam explosion pretreatment of softwood: The effect of the explosive decompression on enzymatic digestibility. *Biotechnol. Biofuels* **2016**, *9*, 152. [[CrossRef](#)]
29. Walker, D.J.; Gallagher, J.; Winters, A.; Somani, A.; Ravella, S.R.; Bryant, D.N. Process Optimization of Steam Explosion Parameters on Multiple Lignocellulosic Biomass Using Taguchi Method—A Critical Appraisal. *Front. Energy Res.* **2018**, *6*, 6. [[CrossRef](#)]
30. Nitsos, C.; Stoklosa, R.; Karnaouri, A.; Vörös, D.; Lange, H.; Hodge, D.; Crestini, C.; Rova, U.; Christakopoulos, P. Isolation and Characterization of Organosolv and Alkaline Lignins from Hardwood and Softwood Biomass. *ACS Sustain. Chem. Eng.* **2016**, *4*, 5181–5193. [[CrossRef](#)]
31. Nitsos, C.; Rova, U.; Christakopoulos, P. Organosolv Fractionation of Softwood Biomass for Biofuel and Biorefinery Applications. *Energies* **2018**, *11*, 50. [[CrossRef](#)]
32. Zhao, X.; Cheng, K.; Liu, D. Organosolv pretreatment of lignocellulosic biomass for enzymatic hydrolysis. *Appl. Microbiol. Biotechnol.* **2009**, *82*, 815–827. [[CrossRef](#)] [[PubMed](#)]
33. Kalogiannis, K.G.; Matsakas, L.; Aspden, J.; Lappas, A.A.; Rova, U.; Christakopoulos, P. Acid Assisted Organosolv Delignification of Beechwood and Pulp Conversion towards High Concentrated Cellulosic Ethanol via High Gravity Enzymatic Hydrolysis and Fermentation. *Molecules* **2018**, *23*, 1647. [[CrossRef](#)] [[PubMed](#)]
34. Matsakas, L.; Nitsos, C.; Raghavendran, V.; Yakimenko, O.; Persson, G.; Olsson, E.; Rova, U.; Olsson, L.; Christakopoulos, P. A novel hybrid organosolv: Steam explosion method for the efficient fractionation and pretreatment of birch biomass. *Biotechnol. Biofuels* **2018**, *11*, 160. [[CrossRef](#)] [[PubMed](#)]

35. Matsakas, L.; Raghavendran, V.; Yakimenko, O.; Persson, G.; Olsson, E.; Rova, U.; Olsson, L.; Christakopoulos, P. Lignin-first biomass fractionation using a hybrid organosolv—Steam explosion pretreatment technology improves the saccharification and fermentability of spruce biomass. *Bioresour. Technol.* **2019**, *273*, 521–528. [[CrossRef](#)] [[PubMed](#)]
36. Margellou, A.; Triantafyllidis, K.S. Catalytic Transfer Hydrogenolysis Reactions for Lignin Valorization to Fuels and Chemicals. *Catalysts* **2019**, *9*, 43. [[CrossRef](#)]
37. Barta, K.; Warner, G.R.; Beach, E.; Anastas, P.T. Depolymerization of organosolv lignin to aromatic compounds over Cu-doped porous metal oxides. *Green Chem.* **2014**, *16*, 191–196. [[CrossRef](#)]
38. Liu, F.; Liu, Q.; Wang, A.; Zhang, T. Direct Catalytic Hydrogenolysis of Kraft Lignin to Phenols in Choline-Derived Ionic Liquids. *ACS Sustain. Chem. Eng.* **2016**, *4*, 3850–3856. [[CrossRef](#)]
39. Onwudili, J.A.; Williams, P.T. Catalytic depolymerization of alkali lignin in subcritical water: Influence of formic acid and Pd/C catalyst on the yields of liquid monomeric aromatic products. *Green Chem.* **2014**, *16*, 4740–4748. [[CrossRef](#)]
40. Molinari, V.; Clavel, G.; Graglia, M.; Antonietti, M.; Esposito, D. Mild Continuous Hydrogenolysis of Kraft Lignin over Titanium Nitride–Nickel Catalyst. *ACS Catal.* **2016**, *6*, 1663–1670. [[CrossRef](#)]
41. Opris, C.; Cojocaru, B.; Gheorghe, N.; Tudorache, M.; Coman, S.M.; Parvulescu, V.I.; Duraki, B.; Krumeich, F.; Van Bokhoven, J.A. Lignin Fragmentation onto Multifunctional Fe₃O₄@Nb₂O₅@Co@Re Catalysts: The Role of the Composition and Deposition Route of Rhenium. *ACS Catal.* **2017**, *7*, 3257–3267. [[CrossRef](#)]
42. Sergeev, A.G.; Hartwig, J.F. Selective, Nickel-Catalyzed Hydrogenolysis of Aryl Ethers. *Science* **2011**, *332*, 439–443. [[CrossRef](#)] [[PubMed](#)]
43. Lazaridis, P.A.; Fotopoulos, A.P.; Karakoulia, S.A.; Triantafyllidis, K.S. Catalytic Fast Pyrolysis of Kraft Lignin With Conventional, Mesoporous and Nanosized ZSM-5 Zeolite for the Production of Alkyl-Phenols and Aromatics. *Front. Chem.* **2018**, *6*, 295. [[CrossRef](#)] [[PubMed](#)]
44. Fox, S.C.; McDonald, A.G. Chemical and Thermal Characterization of Three Industrial Lignins and their Corresponding Lignin Esters. *BioResources* **2010**, *5*, 990–1009.
45. Pandey, M.P.; Kim, C.S. Lignin Depolymerization and Conversion: A Review of Thermochemical Methods. *Chem. Eng. Technol.* **2011**, *34*, 29–41. [[CrossRef](#)]
46. Patwardhan, P.R.; Brown, R.C.; Shanks, B.H. Understanding the Fast Pyrolysis of Lignin. *ChemSusChem* **2011**, *4*, 1629–1636. [[CrossRef](#)] [[PubMed](#)]
47. Jiang, G.; Nowakowski, D.J.; Bridgwater, A.V. Effect of the Temperature on the Composition of Lignin Pyrolysis Products. *Energy Fuels* **2010**, *24*, 4470–4475. [[CrossRef](#)]
48. Vithanage, A.E.; Chowdhury, E.; Alejo, L.D.; Pomeroy, P.C.; DeSisto, W.J.; Frederick, B.G.; Gramlich, W.M. Renewably sourced phenolic resins from lignin bio-oil. *J. Appl. Polym. Sci.* **2017**, *134*, 44827. [[CrossRef](#)]
49. Feghali, E.; Torr, K.M.; Van De Pas, D.J.; Ortiz, P.; Vanbroekhoven, K.; Eevers, W.; Vendamme, R. Thermosetting Polymers from Lignin Model Compounds and Depolymerized Lignins. *Top. Curr. Chem.* **2018**, *376*, 32. [[CrossRef](#)]
50. Bui, V.N.; Laurenti, D.; Afanasiev, P.; Geantet, C. Hydrodeoxygenation of guaiacol with CoMo catalysts. Part I: Promoting effect of cobalt on HDO selectivity and activity. *Appl. Catal. B Environ.* **2011**, *101*, 239–245. [[CrossRef](#)]
51. Mortensen, P.M.; Grunwaldt, J.-D.; Jensen, P.A.; Jensen, A.D. Screening of Catalysts for Hydrodeoxygenation of Phenol as a Model Compound for Bio-oil. *ACS Catal.* **2013**, *3*, 1774–1785. [[CrossRef](#)]
52. Lee, W.-S.; Wang, Z.; Wu, R.J.; Bhan, A. Selective vapor-phase hydrodeoxygenation of anisole to benzene on molybdenum carbide catalysts. *J. Catal.* **2014**, *319*, 44–53. [[CrossRef](#)]
53. De Souza, P.M.; Rabelo-Neto, R.C.; Borges, L.E.P.; Jacobs, G.; Davis, B.H.; Resasco, D.E.; Noronha, F.B. Hydrodeoxygenation of Phenol over Pd Catalysts. Effect of Support on Reaction Mechanism and Catalyst Deactivation. *ACS Catal.* **2017**, *7*, 2058–2073. [[CrossRef](#)]
54. Barrios, A.M.; Teles, C.A.; De Souza, P.M.; Rabelo-Neto, R.C.; Jacobs, G.; Davis, B.H.; Borges, L.E.; Noronha, F.B. Hydrodeoxygenation of phenol over niobia supported Pd catalyst. *Catal. Today* **2018**, *302*, 115–124. [[CrossRef](#)]
55. Resende, K.A.; Teles, C.A.; Jacobs, G.; Davis, B.H.; Cronauer, D.C.; Jeremy Kropf, A.; Marshall, C.L.; Hori, C.E.; Noronha, F.B. Hydrodeoxygenation of phenol over zirconia supported Pd bimetallic catalysts. The effect of second metal on catalyst performance. *Appl. Catal. B Environ.* **2018**, *232*, 213–231. [[CrossRef](#)]
56. Liu, C.; Wang, H.; Karim, A.M.; Sun, J.; Wang, Y. Catalytic fast pyrolysis of lignocellulosic biomass. *Chem. Soc. Rev.* **2014**, *43*, 7594–7623. [[CrossRef](#)]

57. Iliopoulou, E.F.; Lazaridis, P.A.; Triantafyllidis, K.S. Nanocatalysis in the Fast Pyrolysis of Lignocellulosic Biomass. In *Nanotechnology in Catalysis*; Wiley: Hoboken, NJ, USA, 2017; Volume Chapter 27; pp. 655–714.
58. Imran, A.; Bramer, E.A.; Seshan, K.; Brem, G. An overview of catalysts in biomass pyrolysis for production of biofuels. *Biofuel Res. J.* **2018**, *5*, 872–885. [[CrossRef](#)]
59. Rahman, M.M.; Liu, R.; Cai, J. Catalytic fast pyrolysis of biomass over zeolites for high quality bio-oil—A review. *Fuel Process. Technol.* **2018**, *180*, 32–46. [[CrossRef](#)]
60. Iliopoulou, E.F.; Triantafyllidis, K.S.; Lappas, A.A. Overview of catalytic upgrading of biomass pyrolysis vapors toward the production of fuels and high-value chemicals. *Wiley Interdiscip. Rev. Energy Environ.* **2019**, *8*, e322. [[CrossRef](#)]
61. Iliopoulou, E.; Antonakou, E.; Karakoulia, S.; Vasalos, I.; Lappas, A.; Triantafyllidis, K. Catalytic conversion of biomass pyrolysis products by mesoporous materials: Effect of steam stability and acidity of Al-MCM-41 catalysts. *Chem. Eng. J.* **2007**, *134*, 51–57. [[CrossRef](#)]
62. Jae, J.; Tompsett, G.A.; Foster, A.J.; Hammond, K.D.; Auerbach, S.M.; Lobo, R.F.; Huber, G.W. Investigation into the shape selectivity of zeolite catalysts for biomass conversion. *J. Catal.* **2011**, *279*, 257–268. [[CrossRef](#)]
63. Mihalcik, D.J.; Mullen, C.A.; Boateng, A.A. Screening acidic zeolites for catalytic fast pyrolysis of biomass and its components. *J. Anal. Appl. Pyrolysis* **2011**, *92*, 224–232. [[CrossRef](#)]
64. Wang, K.; Kim, K.H.; Brown, R.C. Catalytic pyrolysis of individual components of lignocellulosic biomass. *Green Chem.* **2014**, *16*, 727–735. [[CrossRef](#)]
65. Jackson, M.A.; Compton, D.L.; Boateng, A.A. Screening heterogeneous catalysts for the pyrolysis of lignin. *J. Anal. Appl. Pyrolysis* **2009**, *85*, 226–230. [[CrossRef](#)]
66. Mullen, C.A.; Boateng, A.A. Catalytic pyrolysis-GC/MS of lignin from several sources. *Fuel Process. Technol.* **2010**, *91*, 1446–1458. [[CrossRef](#)]
67. Li, X.; Su, L.; Wang, Y.; Yu, Y.; Wang, C.; Li, X.; Wang, Z. Catalytic fast pyrolysis of Kraft lignin with HZSM-5 zeolite for producing aromatic hydrocarbons. *Front. Environ. Sci. Eng.* **2012**, *6*, 295–303. [[CrossRef](#)]
68. Ma, Z.; Troussard, E.; Van Bokhoven, J.A. Controlling the selectivity to chemicals from lignin via catalytic fast pyrolysis. *Appl. Catal. A Gen.* **2012**, *423*, 130–136. [[CrossRef](#)]
69. Ben, H.; Ragauskas, A.J. Influence of Si/Al Ratio of ZSM-5 Zeolite on the Properties of Lignin Pyrolysis Products. *ACS Sustain. Chem. Eng.* **2013**, *1*, 316–324. [[CrossRef](#)]
70. Zhang, M.; Resende, F.L.; Moutsoglou, A. Catalytic fast pyrolysis of aspen lignin via Py-GC/MS. *Fuel* **2014**, *116*, 358–369. [[CrossRef](#)]
71. Custodis, V.B.F.; Karakoulia, D.S.A.; Triantafyllidis, P.D.K.S.; Van Bokhoven, P.D.J.A. Catalytic Fast Pyrolysis of Lignin over High-Surface-Area Mesoporous Aluminosilicates: Effect of Porosity and Acidity. *ChemSusChem* **2016**, *9*, 1134–1145. [[CrossRef](#)]
72. Serrano, D.P.; Escola, J.M.; Pizarro, P. Synthesis strategies in the search for hierarchical zeolites. *Chem. Soc. Rev.* **2013**, *42*, 4004–4035. [[CrossRef](#)]
73. Park, D.H.; Kim, S.S.; Wang, H.; Pinnavaia, T.J.; Papapetrou, M.C.; Lappas, A.A.; Triantafyllidis, K.S. Selective Petroleum Refining Over a Zeolite Catalyst with Small Intracrystal Mesopores. *Angew. Chem.* **2009**, *121*, 7781–7784. [[CrossRef](#)]
74. Choi, M.; Cho, H.S.; Srivastava, R.; Venkatesan, C.; Choi, D.-H.; Ryoo, R. Amphiphilic organosilane-directed synthesis of crystalline zeolite with tunable mesoporosity. *Nat. Mater.* **2006**, *5*, 718–723. [[CrossRef](#)] [[PubMed](#)]
75. Park, H.J.; Heo, H.S.; Jeon, J.-K.; Kim, J.; Ryoo, R.; Jeong, K.-E.; Park, Y.-K. Highly valuable chemicals production from catalytic upgrading of radiata pine sawdust-derived pyrolytic vapors over mesoporous MFI zeolites. *Appl. Catal. B Environ.* **2010**, *95*, 365–373. [[CrossRef](#)]
76. Kelkar, S.; Saffron, C.M.; Li, Z.; Kim, S.-S.; Pinnavaia, T.J.; Miller, D.J.; Krieger, R. Aromatics from biomass pyrolysis vapour using a bifunctional mesoporous catalyst. *Green Chem.* **2014**, *16*, 803–812. [[CrossRef](#)]
77. Zheng, A.; Zhao, Z.; Chang, S.; Huang, Z.; Wu, H.; Wang, X.; He, F.; Li, H. Effect of crystal size of ZSM-5 on the aromatic yield and selectivity from catalytic fast pyrolysis of biomass. *J. Mol. Catal. A Chem.* **2014**, *383*, 23–30. [[CrossRef](#)]
78. Gamliel, D.P.; Cho, H.J.; Fan, W.; Valla, J.A. On the effectiveness of tailored mesoporous MFI zeolites for biomass catalytic fast pyrolysis. *Appl. Catal. A Gen.* **2016**, *522*, 109–119. [[CrossRef](#)]
79. Hertzog, J.; Carré, V.; Jia, L.; Mackay, C.L.; Pinard, L.; Dufour, A.; Mašek, O.; Aubriet, F. Catalytic Fast Pyrolysis of Biomass over Microporous and Hierarchical Zeolites: Characterization of Heavy Products. *ACS Sustain. Chem. Eng.* **2018**, *6*, 4717–4728. [[CrossRef](#)]

80. Khan, W.; Jia, X.; Wu, Z.; Choi, J.; Yip, A.C. Incorporating Hierarchy into Conventional Zeolites for Catalytic Biomass Conversions: A Review. *Catalysts* **2019**, *9*, 127. [[CrossRef](#)]
81. Fermoso, J.; Hernando, H.; Jana, P.; Moreno, I.; Prech, J.; Ochoa-Hernández, C.; Pizarro, P.; Coronado, J.M.; Čejka, J.; Serrano, D.P. Lamellar and pillared ZSM-5 zeolites modified with MgO and ZnO for catalytic fast-pyrolysis of eucalyptus woodchips. *Catal. Today* **2016**, *277*, 171–181. [[CrossRef](#)]
82. Lee, H.W.; Kim, T.H.; Park, S.H.; Jeon, J.-K.; Suh, D.J.; Park, Y.-K. Catalytic fast pyrolysis of lignin over mesoporous Y zeolite using Py-GC/MS. *J. Nanosci. Nanotechnol.* **2013**, *13*, 2640–2646. [[CrossRef](#)]
83. Li, J.; Li, X.; Zhou, G.; Wang, W.; Wang, C.; Komarneni, S.; Wang, Y. Catalytic fast pyrolysis of biomass with mesoporous ZSM-5 zeolites prepared by desilication with NaOH solutions. *Appl. Catal. A Gen.* **2014**, *470*, 115–122. [[CrossRef](#)]
84. Kim, S.-S.; Lee, H.W.; Ryoo, R.; Kim, W.; Park, S.H.; Jeon, J.-K.; Park, Y.-K. Conversion of kraft lignin over hierarchical MFI zeolite. *J. Nanosci. Nanotechnol.* **2014**, *14*, 2414–2418. [[CrossRef](#)] [[PubMed](#)]
85. Rossberg, C.; Janzon, R.; Saake, B.; Leschinsky, M. Effect of Process Parameters in Pilot Scale Operation on Properties of Organosolv Lignin. *BioResources* **2019**, *14*, 4543–4559.
86. Kalogiannis, K.G.; Matsakas, L.; Lappas, A.A.; Rova, U.; Christakopoulos, P. Aromatics from Beechwood Organosolv Lignin through Thermal and Catalytic Pyrolysis. *Energies* **2019**, *12*, 1606. [[CrossRef](#)]
87. Yáñez-S, M.; Matsuhira, B.; Nuñez, C.; Pan, S.; Hubbell, C.A.; Sannigrahi, P.; Ragauskas, A.J. Physicochemical characterization of ethanol organosolv lignin (EOL) from *Eucalyptus globulus*: Effect of extraction conditions on the molecular structure. *Polym. Degrad. Stab.* **2014**, *110*, 184–194. [[CrossRef](#)]
88. El Mansouri, N.-E.; Salvadó, J. Structural characterization of technical lignins for the production of adhesives: Application to lignosulfonate, kraft, soda-anthraquinone, organosolv and ethanol process lignins. *Ind. Crop. Prod.* **2006**, *24*, 8–16. [[CrossRef](#)]
89. Vishtal, A.G.; Kraslawski, A. Challenges in Industrial Applications of Technical Lignins. *BioResources* **2011**, *6*, 3547–3568.
90. Muraleedharan, M.N.; Zouraris, D.; Karantonis, A.; Topakas, E.; Sandgren, M.; Rova, U.; Christakopoulos, P.; Karnaouri, A. Effect of lignin fractions isolated from different biomass sources on cellulose oxidation by fungal lytic polysaccharide monooxygenases. *Biotechnol. Biofuels* **2018**, *11*, 296. [[CrossRef](#)]
91. Wen, J.-L.; Xue, B.-L.; Sun, S.-L.; Sun, R.-C. Quantitative structural characterization and thermal properties of birch lignins after auto-catalyzed organosolv pretreatment and enzymatic hydrolysis. *J. Chem. Technol. Biotechnol.* **2013**, *88*, 1663–1671. [[CrossRef](#)]
92. Constant, S.; Wienk, H.L.; Frissen, A.E.; de Peinder, P.; Boelens, R.; Van Es, D.S.; Grisel, R.J.; Weckhuysen, B.M.; Huijgen, W.J.; Gosselink, R.J.; et al. New insights into the structure and composition of technical lignins: A comparative characterisation study. *Green Chem.* **2016**, *18*, 2651–2665. [[CrossRef](#)]
93. Crestini, C.; Lange, H.; Sette, M.; Argyropoulos, D.S. On the structure of softwood kraft lignin. *Green Chem.* **2017**, *19*, 4104–4121. [[CrossRef](#)]
94. Ralph, S.A.; Ralph, J.; Landucci, L.L. NMR Database of Lignin and Cell Wall Model Compounds. Available online: www.glbc.org/databases_and_software/nmrdatabase/ (accessed on 10 January 2019).
95. Rencoret, J.; Marques, G.; Gutiérrez, A.; Nieto, L.; Santos, J.I.; Jiménez-Barbero, J.; Martínez, Á.T.; del Río, J.C. HSQC-NMR analysis of lignin in woody (*Eucalyptus globulus* and *Picea abies*) and non-woody (*Agave sisalana*) ball-milled plant materials at the gel state 10th EWLP, Stockholm, Sweden, August 25–28, 2008. *Holzforschung* **2009**, *63*, 691–698. [[CrossRef](#)]
96. Wen, J.L.; Sun, S.L.; Xue, B.L.; Sun, R.C. Recent Advances in Characterization of Lignin Polymer by Solution-State Nuclear Magnetic Resonance (NMR) Methodology. *Materials* **2013**, *6*, 359–391. [[CrossRef](#)] [[PubMed](#)]
97. Yuan, T.-Q.; Sun, S.-N.; Xu, F.; Sun, R.-C. Characterization of Lignin Structures and Lignin–Carbohydrate Complex (LCC) Linkages by Quantitative¹³C and 2D HSQC NMR Spectroscopy. *J. Agric. Food Chem.* **2011**, *59*, 10604–10614. [[CrossRef](#)]
98. Yuan, T.-Q.; Xu, F.; Sun, R.-C. Role of lignin in a biorefinery: Separation characterization and valorization. *J. Chem. Technol. Biotechnol.* **2013**, *88*, 346–352. [[CrossRef](#)]
99. Thommes, M.; Kaneko, K.; Neimark Alexander, V.; Olivier James, P.; Rodriguez-Reinoso, F.; Rouquerol, J.; Sing Kenneth, S.W. *Pure and Applied Chemistry*; de Gruyter: Berlin, Germany, 2015; Volume 87, p. 1051.
100. Groen, J.C.; Moulijn, J.A.; Pérez-Ramírez, J. Desilication: On the controlled generation of mesoporosity in MFI zeolites. *J. Mater. Chem.* **2006**, *16*, 2121–2131. [[CrossRef](#)]

101. Psarras, A.; Michailof, C.; Iliopoulou, E.; Kalogiannis, K.; Lappas, A.; Heracleous, E.; Triantafyllidis, K. Acetic acid conversion reactions on basic and acidic catalysts under biomass fast pyrolysis conditions. *Mol. Catal.* **2019**, *465*, 33–42. [[CrossRef](#)]
102. Komvokis, V.; Karakoulia, S.; Iliopoulou, E.; Papapetrou, M.; Vasalos, I.; Lappas, A.; Triantafyllidis, K. Upgrading of Fischer–Tropsch synthesis bio-waxes via catalytic cracking: Effect of acidity, porosity and metal modification of zeolitic and mesoporous aluminosilicate catalysts. *Catal. Today* **2012**, *196*, 42–55. [[CrossRef](#)]
103. Triantafyllidis, K.S.; Nalbandian, L.; Trikalitis, P.N.; Ladavos, A.K.; Mavromoustakos, T.; Nicolaides, C.P. Structural, compositional and acidic characteristics of nanosized amorphous or partially crystalline ZSM-5 zeolite-based materials. *Microporous Mesoporous Mater.* **2004**, *75*, 89–100. [[CrossRef](#)]
104. Triantafyllidis, C.S.; Vlessidis, A.G.; Nalbandian, L.; Evmiridis, N.P. Effect of the degree and type of the dealumination method on the structural, compositional and acidic characteristics of H-ZSM-5 zeolites. *Microporous Mesoporous Mater.* **2001**, *47*, 369–388. [[CrossRef](#)]
105. Lin, X.; Sui, S.; Tan, S.; Pittman, C.U.; Sun, J.; Zhang, Z. Fast Pyrolysis of Four Lignins from Different Isolation Processes Using Py-GC/MS. *Energies* **2015**, *8*, 5107–5121. [[CrossRef](#)]
106. Kalogiannis, K.G.; Stefanidis, S.D.; Michailof, C.M.; Lappas, A.A.; Sjöholm, E. Pyrolysis of lignin with 2DGC quantification of lignin oil: Effect of lignin type, process temperature and ZSM-5 in situ upgrading. *J. Anal. Appl. Pyrolysis* **2015**, *115*, 410–418. [[CrossRef](#)]
107. Yang, H.; Appari, S.; Kudo, S.; Hayashi, J.-I.; Kumagai, S.; Norinaga, K. Chemical Structures and Primary Pyrolysis Characteristics of Lignins Obtained from Different Preparation Methods. *J. Jpn. Inst. Energy* **2014**, *93*, 986–994. [[CrossRef](#)]
108. Yu, Y.; Li, X.; Su, L.; Zhang, Y.; Wang, Y.; Zhang, H. The role of shape selectivity in catalytic fast pyrolysis of lignin with zeolite catalysts. *Appl. Catal. A Gen.* **2012**, *447*, 115–123. [[CrossRef](#)]
109. Kawamoto, H. Lignin pyrolysis reactions. *J. Wood Sci.* **2017**, *63*, 117–132. [[CrossRef](#)]
110. Hemberger, P.; Custodis, V.B.F.; Bodi, A.; Gerber, T.; Van Bokhoven, J.A. Understanding the mechanism of catalytic fast pyrolysis by unveiling reactive intermediates in heterogeneous catalysis. *Nat. Commun.* **2017**, *8*, 15946. [[CrossRef](#)]
111. Chu, S.; Subrahmanyam, A.V.; Huber, G.W. The pyrolysis chemistry of a β -O-4 type oligomeric lignin model compound. *Green Chem.* **2013**, *15*, 125–136. [[CrossRef](#)]
112. Custodis, V.B.F.; Hemberger, P.; Van Bokhoven, J.A.; Hemberger, D.P.; Van Bokhoven, P.D.J.A. How Inter- and Intramolecular Reactions Dominate the Formation of Products in Lignin Pyrolysis. *Chem.-A Eur. J.* **2017**, *23*, 8658–8668. [[CrossRef](#)]
113. Neumann, G.T.; Pimentel, B.R.; Rensel, D.J.; Hicks, J.C. Correlating lignin structure to aromatic products in the catalytic fast pyrolysis of lignin model compounds containing β -O-4 linkages. *Catal. Sci. Technol.* **2014**, *4*, 3953–3963. [[CrossRef](#)]
114. Jiang, X.; Lu, Q.; Hu, B.; Liu, J.; Dong, C.; Yang, Y. A Comprehensive Study on Pyrolysis Mechanism of Substituted β -O-4 Type Lignin Dimers. *Int. J. Mol. Sci.* **2017**, *18*, 2364. [[CrossRef](#)]
115. Stephanidis, S.; Nitsos, C.; Kalogiannis, K.; Iliopoulou, E.; Lappas, A.; Triantafyllidis, K. Catalytic upgrading of lignocellulosic biomass pyrolysis vapours: Effect of hydrothermal pre-treatment of biomass. *Catal. Today* **2011**, *167*, 37–45. [[CrossRef](#)]
116. Zhou, G.; Jensen, P.A.; Le, D.M.; Knudsen, N.O.; Jensen, A.D. Direct upgrading of fast pyrolysis lignin vapor over the HZSM-5 catalyst. *Green Chem.* **2016**, *18*, 1965–1975. [[CrossRef](#)]
117. Lee, H.W.; Kim, Y.-M.; Jae, J.; Sung, B.H.; Jung, S.-C.; Kim, S.C.; Jeon, J.-K.; Park, Y.-K. Catalytic pyrolysis of lignin using a two-stage fixed bed reactor comprised of in-situ natural zeolite and ex-situ HZSM-5. *J. Anal. Appl. Pyrolysis* **2016**, *122*, 282–288. [[CrossRef](#)]
118. Heikkinen, S.; Toikka, M.M.; Karhunen, P.T.; Kilpeläinen, I.A. Quantitative 2D HSQC (Q-HSQC) via Suppression of β -Dependence of Polarization Transfer in NMR Spectroscopy: Application to Wood Lignin. *J. Am. Chem. Soc.* **2003**, *125*, 4362–4367. [[CrossRef](#)]

